Directional Compactly Supported Tensor Product Complex Tight Framelets with Applications to Image Denoising and Inpainting[*]

Bin Han[†], Qun Mo[‡], Zhenpeng Zhao[†], and Xiaosheng Zhuang[§]

Abstract. Compactly supported tight framelets are of great interest and importance in both theory and application. In this paper we discuss how to construct directional compactly supported tensor product complex tight framelets having varied directionality and good performance for applications in image processing. Our construction algorithms employ optimization techniques and put extensive emphasis on frequency response and spatial localization of their underlying one-dimensional tight framelet filter banks. Several concrete examples of directional compactly supported tensor product complex tight framelet filter banks are provided in this paper. Our numerical experiments show that such constructed directional compactly supported tensor product complex tight framelets have good performance for applications such as image denoising and inpainting compared with several other state-of-the-art transform-based methods.

Key words. complex tight framelets, directionality, tensor product, complex-valued framelet filter banks, image denoising and inpainting, frequency separation property, compactly supported framelets

AMS subject classifications. 41A25, 42B05, 42C40, 42C15, 65T60, 68U10, 68W35, 68W40, 94A12, 94A08

DOI. 10.1137/19M1249734

1. Introduction and motivations. Transform-based image processing including denoising and inpainting plays a crucial role in many real-life applications such as medical imaging (MRI, CT, PET, etc.), remote sensing, and astrology, seismology, neuroimaging, and so on [3, 31, 33, 39, 41]. Sparsity is the key for the successful applications of various approaches where sparsity is captured by suitable representation systems. It has been shown that for a large class of images modeled by "cartoon-like" functions, directional multiscale representation systems such as *curvelets* and *shearlets* can provide (nearly) optimal sparse representation [2, 29]. Directionality is no doubt one of the most important features of a multiscale representation system.

[†]Department of Mathematical and Statistical Sciences, University of Alberta, Edmonton, Alberta T6G 2G1, Canada (bhan@ualberta.ca, zzhao7@ualberta.ca, http://www.ualberta.ca/~bhan).

[‡]School of Mathematical Sciences, Zhejiang University, Hangzhou 310027, People's Republic of China (moqun@zju.edu.cn).

[§]Department of Mathematics, City University of Hong Kong, Tat Chee Avenue, Kowloon Tong, Hong Kong (xzhuang7@cityu.edu.hk, http://staffweb1.cityu.edu.hk/xzhuang7).

(a) DB   (b) $\mathbb{C}\text{TF}_3$ (c) $\mathbb{C}\text{TF}_4$ (d) $\mathbb{C}\text{TF}_5$ (e) $\mathbb{C}\text{TF}_6$
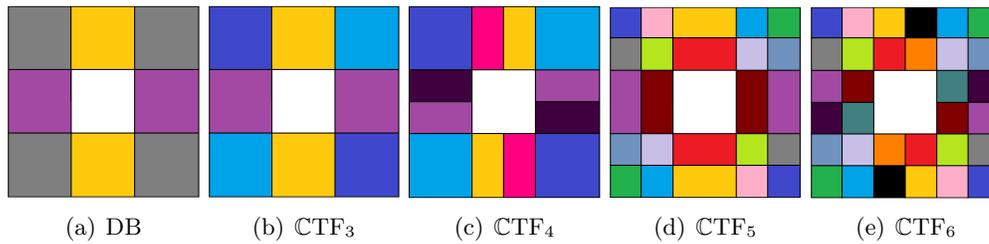
Figure 1. *Illustration of frequency tilings of tensor product systems using* (a) *Daubechies orthogonal wavelet filter bank* $\text{DB} = \{a; b\}$, *and complex tight framelet filter banks:* (b) $\mathbb{C}\text{TF}_3 = \{a; b^+, b^-\}$, (c) $\mathbb{C}\text{TF}_4 = \{a^+, a^-; b^+, b^-\}$, (d) $\mathbb{C}\text{TF}_5 = \{a; b_1^+, b_1^-, b_2^+, b_2^-\}$, *and* (e) $\mathbb{C}\text{TF}_6 = \{a^+, a^-; b_1^+, b_1^-, b_2^+, b_2^-\}$. *The (big) square in each subfigure represents the frequency domain* $\mathbb{T}^2 = [-\pi, \pi)^2$. *The middle white block is the tiling of the low-pass filter while each colored block corresponds to a directional high-pass filter. The tilings with respect to* $\mathbb{C}\text{TF}_4$ *are similar to the tilings of the dual tree complex wavelet transform (*DT-$\mathbb{C}$WT*) in* [28, 37]. *The numbers of (effective) directions in* (a)–(e) *are* $2, 4, 6, 8, 14$, *respectively.*

Curvelets or shearlets are usually band-limited tight frame systems [2, 14, 15]. They are typically constructed through a nontensor product approach in the sense that the curvelet or shearlet system in higher dimension cannot be obtained simply through the tensor product of an underlying one-dimensional system. The goal of this paper is to construct spatially compactly supported tight framelets. On the one hand, since the invention of compactly supported real-valued orthogonal wavelets by Daubechies [9], development of compactly supported wavelet/framelet systems has been one of the main themes in wavelet analysis and applications [7, 10, 16, 36]. For high-dimensional problems, the tensor product approach provides a simple and efficient way for the construction of multidimensional wavelet systems. On the other hand, it is well known that tensor product *real-valued* wavelets lack directionality in practice. In fact, for a Daubechies orthogonal wavelet filter bank $\text{DB} = \{a; b\}$, where a, b are the low- and high-pass real-valued filters, respectively, the energy of the low-pass filter a in the frequency domain $\mathbb{T} := [-\pi, \pi)$ is concentrated near the origin, while for the high-pass filter b it is concentrated away from the origin. In such a case, the tensor product Daubechies orthogonal wavelet filter bank in two dimensions (2D) is $\{a \otimes a; a \otimes b, b \otimes a, b \otimes b\}$, which only favors the horizontal direction (via $a \otimes b$) and the vertical direction (via $b \otimes a$); see Figure 1(a) for its frequency tiling and note that the checkerboard filter $b \otimes b$ has no directionality. Of course, to achieve more directionality, one can abandon the tensor product approach and turn to the nontensor product approaches as those in curvelet- and shearlet-like systems [1, 3, 5, 18, 26, 35, 42]. However, in view of its simplicity and efficiency when facing high-dimensional problems (image, video, etc.), we restrict ourselves in this paper to the tensor product approach for the construction of directional systems.

To achieve more directionality based on the tensor product approach, one can consider *complex-valued* framelet systems instead of real-valued wavelet systems. The main idea is very simple. Taking complex tight framelet filter bank (see section 2) $\mathbb{C}\text{TF}_3 = \{a; b^+, b^-\}$ for example, one first designs a (complex-valued) high-pass filter b^+ with its frequency response mainly in the positive part of $\mathbb{T}$. Then, a filter b^- defined by $b^- := \overline{b^+}$ gives rise to a (complex-valued) high-pass filter with its frequency response mainly in the negative part of $\mathbb{T}$. The tensor product of $\mathbb{C}\text{TF}_3$ in 2D produces a filter bank $\{a \otimes a; a \otimes b^\pm, b^\pm \otimes a, b^\pm \otimes b^\pm\}$ with

(a) Table cloth   (b) $\sigma = 25$ (c) DB (27.18)   (d) $\mathbb{C}\mathrm{TF}_3$ (28.01) (e) $\mathbb{C}\mathrm{TF}_6$ (29.25)
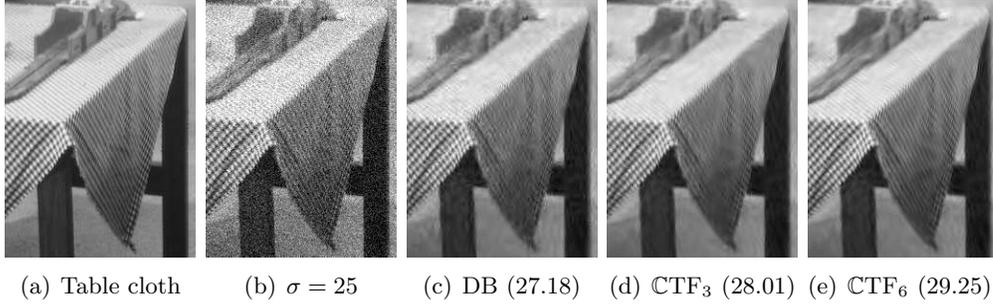
Figure 2. *Denoising comparison. (a) Cropped image from* `Barbara`*. (b) Noisy image with white Gaussian noise ($\sigma = 25$). (c) Denoised by* DB *(db4). (d) Denoised by compactly supported* $\mathbb{C}\mathrm{TF}_3$*. (e) Denoised by compactly supported* $\mathbb{C}\mathrm{TF}_6$*. The numbers* 27.18, 28.01, *and* 29.25 *are the peak signal-to-noise ratio (PSNR) values of the denoised image using* DB, $\mathbb{C}\mathrm{TF}_3$*, and* $\mathbb{C}\mathrm{TF}_6$*, respectively.*

9 filters and 4 directions, where $a \otimes b^+$ and $b^+ \otimes a$ are with respect to horizontal and vertical directions ($\pm 90°$) while $b^+ \otimes b^+$ and $b^- \otimes b^+$ are with respect to the diagonal and antidiagonal directions ($\pm 45°$); see Figure 1(b) for its frequency tiling. We also point out that the complex orthonormal wavelets in [17] have symmetry but lack directionality.

Using the splitting technique which we detail later in section 3, we can obtain a filter bank $\mathbb{C}\mathrm{TF}_4 = \{a^+, a^-; b^+, b^-\}$ by splitting the low-pass filter a in $\mathbb{C}\mathrm{TF}_3$ to two low-pass filters a^+, a^- whose frequency responses are mainly near the positive origin $[0, \varepsilon]$ and the negative origin $[-\varepsilon, 0]$ of $\mathbb{T}$ for some $\varepsilon > 0$, respectively. Then the tensor product of $\mathbb{C}\mathrm{TF}_4$ in 2D gives a filter bank $\{a \otimes a; a^\pm \otimes b^\pm, b^\pm \otimes a^\pm, b^\pm \otimes b^\pm\}$ with 13 filters and 6 directions ($\pm 15°, \pm 45°, \pm 75°$; see Figure 1(c) for its frequency tiling and note that we use the original low-pass filter $a \otimes a$ instead of $a^\pm \otimes a^\pm$). Such a system is indeed similar to the DT-$\mathbb{C}$WT proposed in [28, 37]. Splitting b^+ into two high-pass filters b_1^+, b_2^+ as well as defining $b_1^- := \overline{b_1^+}, b_2^- := \overline{b_2^+}$ can produce complex tight framelet filter banks $\mathbb{C}\mathrm{TF}_5 := \{a; b_1^+, b_1^-, b_2^+, b_2^-\}$ and $\mathbb{C}\mathrm{TF}_6 := \{a^+, a^-; b_1^+, b_1^-, b_2^+, b_2^-\}$. The tensor product of $\mathbb{C}\mathrm{TF}_5$ in 2D has 25 filters and 8 directions while the tensor product of $\mathbb{C}\mathrm{TF}_6$ in 2D has 33 filters and 14 directions. See Figure 1(d)–(e) for their frequency tilings.

With more directionality, it brings more performance improvement in practice. Figure 2 gives a comparison in image denoising using such $\mathbb{C}\mathrm{TF}_n$ systems as developed in this paper. One can see that the image in Figure 2(a) (cropped from `Barbara`) corrupted by white Gaussian noise with $\sigma = 25$ loses many directional features in Figure 2(b). As expected, the denoised image by the tensor product Daubechies orthogonal wavelet filter bank (DB) in Figure 2(c) does not recover much detail with respect to the directional patterns on the table cloth while $\mathbb{C}\mathrm{TF}_3$ and $\mathbb{C}\mathrm{TF}_6$ can recover more details on the table cloth than that of DB. Moreover, $\mathbb{C}\mathrm{TF}_6$ clearly performs better than both DB and $\mathbb{C}\mathrm{TF}_3$ due to its rich directionality (see section 5 for more details on image denoising).

A family of directional tensor product complex tight framelets (TP-$\mathbb{C}$TFs) following the above idea has been introduced in [19] and further developed in [24, 25]. Experimental results demonstrate that TP-$\mathbb{C}$TFs have significantly better performance than many other transform-based methods for the model problems of image denoising in [24], image inpainting in [39], and video denoising/inpainting in [25]. However, the TP-$\mathbb{C}$TFs constructed in [19, 24, 25] are

band limited (we thus term them $\text{TP}^b\text{-}\mathbb{C}\text{TF}_n$ with b standing for band limited). Hence, in the spatial/time domain, they cannot have compact support. Since *compactly supported* wavelets or framelets have good space-frequency localization and lead to efficient computational algorithms, they are of great importance both theoretically and practically. The initial effort on finding directional compactly supported TP-CTFs, which we term $\text{TP}^c\text{-}\mathbb{C}\text{TF}_n$ in this paper in comparison to its band-limited counterpart $\text{TP}^b\text{-}\mathbb{C}\text{TF}_n$ in [19, 24, 25], has been started in [23], which concentrates on the *simplest* directional compactly supported $\text{TP}^c\text{-}\mathbb{C}\text{TF}_3$ with only two high-pass filters in one dimension.

In this paper we are interested in constructing *directional compactly supported* $\text{TP}^c\text{-}\mathbb{C}\text{TF}_n$ with $n = 3, 4, 5, 6$ and good performance for applications such as image denoising and image inpainting. It is necessary to point out here that finding concrete good examples of directional compactly supported $\text{TP}^c\text{-}\mathbb{C}\text{TF}_n$, though it appears to be easy and trivial, is one of the most difficult tasks in this paper. For example, one problem that we are facing is what kinds of low-pass filters are suitable for constructing directional compactly supported $\text{TP}^c\text{-}\mathbb{C}\text{TF}_n$ such that they have superior performance for practical applications. Though the low-pass filters for the *B*-spline functions and Daubechies orthogonal wavelets in [9] are very popular and widely used in the literature of wavelet analysis, as we explain in this paper, they are not suitable for our purpose. Indeed, directional compactly supported $\text{TP}^c\text{-}\mathbb{C}\text{TF}_n$ with $n = 3, 4, 5, 6$ can also be constructed from these low-pass *B*-spline filters by our algorithms, but they do not perform that well in the image denoising/inpainting problem.

The contributions of this paper lie in the following aspects. First, we provide step-by-step algorithms for the construction of directional compactly supported $\text{TP}^c\text{-}\mathbb{C}\text{TF}_n$ by utilizing both theoretical analysis and optimization techniques. Second, we define a quantity to measure the frequency separation property of a filter, based on which the frequency separation ability of the families of Daubechies orthogonal wavelet filters, interpolatory filters, and *B*-spline filters can be studied. More importantly, a suitable new family of low-pass filters can be built for the construction of compactly supported $\mathbb{C}\text{TF}_n$ with good performance. Third, we provide concrete examples of compactly supported $\mathbb{C}\text{TF}_n$ for $n = 3, 4, 5, 6$ and demonstrate the effectiveness of such compactly supported $\mathbb{C}\text{TF}_n$ in image denoising and image inpainting. Last but not least, the design of band-limited $\mathbb{C}\text{TF}_n$ in [19, 24, 25] together with the design of compactly supported $\mathbb{C}\text{TF}_n$ in this paper gives a complete picture on the analysis, construction, and applications of $\mathbb{C}\text{TF}_n$ in both band-limited and compactly supported settings. We also point out that our constructed compactly supported $\mathbb{C}\text{TF}_n$ also offer the possibility of being adapted to bounded intervals with high vanishing moments. As a consequence, their performance in applications such as image processing may be further improved by reducing the boundary artifacts and improved sparsity near boundaries. Due to the complexity of adapting framelets to bounded intervals, we shall leave this topic as a future research problem, while in this paper we mainly concentrate on developing the necessary theory and algorithms for constructing compactly supported $\mathbb{C}\text{TF}_n$ with directionality.

The structure of this paper is as follows. In section 2, we briefly recall the construction of directional band-limited $\text{TP}^b\text{-}\mathbb{C}\text{TF}_n$ with $n \geqslant 3$, and discuss the frequency separation property of a filter. In section 3, we study how to split a finitely supported low-pass filter a into two finitely supported auxiliary filters a^+ and a^- with good frequency separation properties. Then we study particular low-pass filters which are used in our construction of directional compactly

supported $\text{TP}^c\text{-}\mathbb{CTF}_n$ with $n = 3, 4, 5, 6$ for image processing. In section 4, we provide step-by-step algorithms for constructing compactly supported $\mathbb{CTF}_n$ with $n = 3, 4, 5, 6$ having good frequency separation property with prescribed filter supports. Several concrete numerical examples are given to illustrate our construction algorithms in section 4. Finally, in section 5, we test our directional compactly supported $\text{TP}^c\text{-}\mathbb{CTF}_n$ with $n = 3, 4, 5, 6$ in image denoising and inpainting by comparing the performance with their band-limited counterparts as well as other state-of-the-art transform-based methods. Conclusions and further remarks are given in section 6. Proofs of some theorems are postponed to section 7.

2. Preliminaries on tensor product complex tight framelets. To prepare for the construction of directional compactly supported $\text{TP}^c\text{-}\mathbb{CTF}_n$ with $n \in \{3, 4, 5, 6\}$, in this section we briefly review tight framelets and tight framelet filter banks and the construction of directional band-limited $\text{TP}^b\text{-}\mathbb{CTF}_n$ with $n \geqslant 3$ in [19, 24, 25].

2.1. Tight framelet filter banks and tight framelets in $\boldsymbol{L_2(\mathbb{R}^d)}$. A d-dimensional *filter* $u := \{u(k)\}_{k \in \mathbb{Z}^d}$ is a sequence of complex numbers defined on $\mathbb{Z}^d$. By $u \in l_0(\mathbb{Z}^d)$ we mean that u is a sequence on $\mathbb{Z}^d$ having finite support. For $1 \leqslant p < \infty$, we say that $u = \{u(k)\}_{k \in \mathbb{Z}^d} \in l_p(\mathbb{Z}^d)$ if $\|u\|_{l_p(\mathbb{Z}^d)}^p := \sum_{k \in \mathbb{Z}^d} |u(k)|^p < \infty$. For $u = \{u(k)\}_{k \in \mathbb{Z}^d} \in l_2(\mathbb{Z}^d)$, we define its Fourier series (or symbol) to be $\widehat{u}(\xi) := \sum_{k \in \mathbb{Z}^d} u(k) e^{-ik \cdot \xi}$, $\xi \in \mathbb{R}^d$. For a one-dimensional filter $u \in l_0(\mathbb{Z})$, we define its filter support $\operatorname{fsupp}(u) := [m, n]$ and filter length $\operatorname{len}(u) := n - m$, where $u(m)u(n) \neq 0$ and $u(k) = 0$ for all $k \in \mathbb{Z} \backslash [m, n]$. We often list a filter u by $u = \{u(m), \ldots, u(n)\}_{[m,n]}$.

For $a, b_1, \ldots, b_s \in l_2(\mathbb{Z}^d)$, we say that $\{a; b_1, \ldots, b_s\}$ is a (d-dimensional dyadic) *tight framelet filter bank* if

$$(2.1) \qquad |\widehat{a}(\xi)|^2 + \sum_{\ell=1}^s |\widehat{b_\ell}(\xi)|^2 = 1 \quad \text{and} \quad \widehat{a}(\xi)\overline{\widehat{a}(\xi + \pi\omega)} + \sum_{\ell=1}^s \widehat{b_\ell}(\xi)\overline{\widehat{b_\ell}(\xi + \pi\omega)} = 0$$

for $\omega \in ([0,1]^d \cap \mathbb{Z}^d) \backslash \{0\}$ and for almost every $\xi \in \mathbb{R}^d$. Moreover, a (d-dimensional dyadic) tight framelet filter bank $\{a; b_1, \ldots, b_s\}$ is called a (d-dimensional dyadic) *orthogonal wavelet filter bank* when $s = 2^d - 1$.

If there exist positive numbers C and τ such that $|\widehat{a}(\xi) - 1| \leqslant C|\xi|^\tau$ for all $\xi \in [-\pi, \pi)^d$ (this condition is automatically satisfied if $a \in l_0(\mathbb{Z}^d)$ and $\widehat{a}(0) = 1$), then the following functions are well defined for a tight framelet filter bank $\{a; b_1, \ldots, b_s\}$:

$$\widehat{\phi}(\xi) := \prod_{j=1}^{\infty} \widehat{a}(2^{-j}\xi) \quad \text{and} \quad \widehat{\psi_\ell}(\xi) := \widehat{b_\ell}(\xi/2)\widehat{\phi}(\xi/2), \qquad \xi \in \mathbb{R}^d, \ \ell = 1, \ldots, s,$$

where the Fourier transform is defined to be $\widehat{f}(\xi) := \int_{\mathbb{R}^d} f(x) e^{-ix \cdot \xi} dx$ for $f \in L_1(\mathbb{R}^d)$. Then it is known from [18, Theorem 17 and Corollary 12] that $\{\phi; \psi_1, \ldots, \psi_s\}$ is a tight framelet for $L_2(\mathbb{R}^d)$, that is,

$$\|f\|_{L_2(\mathbb{R}^d)}^2 = \sum_{k \in \mathbb{Z}^d} |\langle f, \phi(\cdot - k)\rangle|^2 + \sum_{j=0}^{\infty} \sum_{\ell=1}^s \sum_{k \in \mathbb{Z}^d} |\langle f, 2^{dj/2}\psi^\ell(2^j \cdot - k)\rangle|^2 \qquad \text{for all } f \in L_2(\mathbb{R}^d).$$

If $a \in l_0(\mathbb{Z}^d)$ with $\widehat{a}(0) = 1$, then $\{\phi; \psi_1, \ldots, \psi_s\}$ is a tight framelet for $L_2(\mathbb{R}^d)$ if and only if $\{a; b_1, \ldots, b_s\}$ is a tight framelet filter bank (for more details on framelets and framelet filter banks, we refer to the book [22]). As a consequence, in this paper we mainly concentrate on tight framelet filter banks instead of tight framelets for $L_2(\mathbb{R}^d)$.

A d-dimensional dyadic tight framelet filter bank can be easily obtained through the tensor product of a one-dimensional tight framelet filter bank. For filters $u_1, \ldots, u_d \in l_1(\mathbb{Z})$ in one dimension, we define their d-dimensional tensor product filter $u_1 \otimes \cdots \otimes u_d$ to be $(u_1 \otimes \cdots \otimes u_d)(k_1, \ldots, k_d) := u_1(k_1) \cdots u_d(k_d)$ for $k_1, \ldots, k_d \in \mathbb{Z}$. In particular, we define $\otimes^d u := u \otimes \cdots \otimes u$ as the tensor product of d copies of u. If $\{a; b_1, \ldots, b_s\}$ is a one-dimensional tight framelet filter bank, then it is straightforward to check that $\otimes^d \{a; b_1, \ldots, b_s\}$ is a d-dimensional tight framelet filter bank with the d-dimensional low-pass filter $\otimes^d a$.

2.2. Directional band-limited tensor product complex tight framelets. We now briefly recall the construction of directional band-limited $\mathrm{TP}^b\text{-}\mathbb{C}\mathrm{TF}_n$ in [19, 24, 25]. For $c_L < c_R$ and two positive numbers $\varepsilon_L, \varepsilon_R$ satisfying $\varepsilon_L + \varepsilon_R \leqslant c_R - c_L$, we define a bump function $\chi_{[c_L, c_R]; \varepsilon_L, \varepsilon_R}$ on $\mathbb{R}$ [16, 19, 24, 25] by

$$\chi_{[c_L, c_R]; \varepsilon_L, \varepsilon_R}(\xi) := \begin{cases} 0, & \xi \leqslant c_L - \varepsilon_L \text{ or } \xi \geqslant c_R + \varepsilon_R, \\ \sin\left(\frac{\pi}{2} \mathsf{Q}_m\left(\frac{c_L + \varepsilon_L - \xi}{2\varepsilon_L}\right)\right), & c_L - \varepsilon_L < \xi < c_L + \varepsilon_L, \\ 1, & c_L + \varepsilon_L \leqslant \xi \leqslant c_R - \varepsilon_R, \\ \sin\left(\frac{\pi}{2} \mathsf{Q}_m\left(\frac{\xi - c_R + \varepsilon_R}{2\varepsilon_R}\right)\right), & c_R - \varepsilon_R < \xi < c_R + \varepsilon_R, \end{cases}$$

where $\mathsf{Q}_m(x) := (1-x)^m \sum_{j=0}^{m-1} \binom{m+j-1}{j} x^j$ satisfying $\mathsf{Q}_m(x) + \mathsf{Q}_m(1-x) = 1$ (see [9]). For simplicity, we take $m = 1$ (that is, $\mathsf{Q}_1(x) = 1 - x$) throughout this paper. Let $s \in \mathbb{N}$ and $0 < c_1 < c_2 < \cdots < c_{s+1} := \pi$ and $\varepsilon_0, \varepsilon_1, \ldots, \varepsilon_{s+1}$ be positive real numbers satisfying

$$0 < \varepsilon_0 < c_1 - \varepsilon_1, \quad 0 < \varepsilon_1 \leqslant \min(c_1, \tfrac{\pi}{2} - c_1), \quad \text{and} \quad (c_{\ell+1} - c_\ell) + \varepsilon_{\ell+1} + \varepsilon_\ell \leqslant \pi, \qquad \ell = 1, \ldots, s.$$

The filters $a, b_1^+, \ldots, b_s^+, b_1^-, \ldots, b_s^-$ are defined through their 2π-periodic Fourier series on the fundamental interval $\mathbb{T} = [-\pi, \pi)$ as follows:

$$(2.2) \qquad \widehat{a} := \chi_{[-c_1, c_1]; \varepsilon_1, \varepsilon_1}, \quad \widehat{b_\ell^+} := \chi_{[c_\ell, c_{\ell+1}]; \varepsilon_\ell, \varepsilon_{\ell+1}}, \quad \text{and} \quad \widehat{b_\ell^-} := \overline{\widehat{b_\ell^+}(-\cdot)}, \qquad \ell = 1, \ldots, s.$$

Then $\mathbb{C}\mathrm{TF}_{2s+1} := \{a; b_1^+, \ldots, b_s^+, b_1^-, \ldots, b_s^-\}$ is a (one-dimensional dyadic) tight framelet filter bank with total $(2s+1)$ one-dimensional filters. The *directional band-limited tensor product complex tight framelet filter bank* $\mathrm{TP}^b\text{-}\mathbb{C}\mathrm{TF}_{2s+1}$ in dimension d is given by

$$\mathrm{TP}^b\text{-}\mathbb{C}\mathrm{TF}_{2s+1} := \otimes^d \mathbb{C}\mathrm{TF}_{2s+1} = \otimes^d \{a; b_1^+, \ldots, b_s^+, b_1^-, \ldots, b_s^-\}.$$

This family of tensor product complex tight framelet filter banks has been introduced in [19].

To further improve the directionality of $\mathrm{TP}^b\text{-}\mathbb{C}\mathrm{TF}_{2s+1}$, another closely related family of directional band-limited tensor product complex tight framelet filter banks $\mathrm{TP}^b\text{-}\mathbb{C}\mathrm{TF}_{2s+2}$ has been introduced in [24]. Let $0 < \varepsilon_0 < c_1 - \varepsilon_1$. Define filters $a, b_1^+, \ldots, b_s^+, b_1^-, \ldots, b_s^-$ as in (2.2), and define two auxiliary complex-valued filters a^+ and a^- by

$$(2.3) \qquad \widehat{a^+} := \chi_{[0, c_1]; \varepsilon_0, \varepsilon_1}, \qquad \widehat{a^-} := \overline{\widehat{a^+}(-\cdot)}.$$
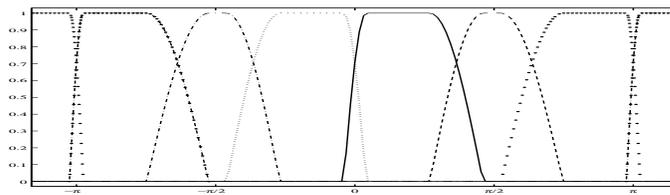
Figure 3. *An example of* $\mathbb{CTF}_6 = \{a^+, a^-; b_1^+, b_2^+, b_1^-, b_2^-\}$. *Middle 2:* $\widehat{a^+}$ *(Solid line) and* $\widehat{a^-}$ *(dotted line).* *Left:* $\widehat{b_2^-}$ *(circle-dotted line) and* $\widehat{b_1^-}$ *(dash-dotted line).* *Right:* $\widehat{b_1^+}$ *(dashed line) and* $\widehat{b_2^+}$ *(circled line).*

Then $\mathbb{CTF}_{2s+2} := \{a^+, a^-; b_1^+, \ldots, b_s^+, b_1^-, \ldots, b_s^-\}$ is a (one-dimensional dyadic) tight framelet filter bank with total $(2s+2)$ one-dimensional filters. See Figure 3 for an illustration of such a $\mathbb{CTF}_{2s+2}$ with $s = 2$. Now the directional band-limited tensor product complex tight framelet filter bank $\text{TP}^b\text{-}\mathbb{CTF}_{2s+2}$ in d dimensions is defined to be

$$\text{TP}^b\text{-}\mathbb{CTF}_{2s+2} := \{\otimes^d a; \text{TP}^b\text{-}\mathbb{CTF}\text{-}\text{HP}_{2s+2}\},$$

where $\text{TP}^b\text{-}\mathbb{CTF}\text{-}\text{HP}_{2s+2} := (\otimes^d\{a^+, a^-; b_1^+, \ldots, b_s^+, b_1^-, \ldots, b_s^-\})\backslash(\otimes^d\{a^+, a^-\})$. See [19, 23, 24, 25, 39] for detailed discussions on tensor product complex tight framelets and their applications to image/video processing. Due to the last identities in (2.2) and (2.3), it is important to notice that

$$a^- = \overline{a^+}, \quad b_1^- = \overline{b_1^+}, \quad \ldots, \quad b_s^- = \overline{b_s^+},$$

where $\overline{u}(k) := \overline{u(k)}, k \in \mathbb{Z}$, or, equivalently, $\widehat{\overline{u}}(\xi) := \overline{\widehat{u}(-\xi)}$.

2.3. Directionality and frequency separation property. The above constructed directional band-limited $\text{TP}^b\text{-}\mathbb{CTF}_n$ with $n \geqslant 3$ are band limited and do not have compact support in the spatial domain. In view of the importance of compactly supported tensor product complex tight framelets in both theory and application, it is highly desirable to know whether it is possible to construct directional compactly supported $\text{TP}^c\text{-}\mathbb{CTF}_n$ with good performance in practical applications over other state-of-the-art transform-based methods in the literature.

The paper [23] is the first one to pursue this goal by studying directional compactly supported $\text{TP}^c\text{-}\mathbb{CTF}_3$. However, $\text{TP}^c\text{-}\mathbb{CTF}_3$ often performs inferior in applications (due to lack of a sufficient number of directions) compared with $\text{TP}^b\text{-}\mathbb{CTF}_4$ or $\text{TP}^b\text{-}\mathbb{CTF}_6$. Moreover, the several constructed examples of $\text{TP}^c\text{-}\mathbb{CTF}_3$ in [23] are of only theoretical interest and do not perform very well for image processing, due to several factors that we address later in this paper. Therefore, it is necessary and important for us to study directional compactly supported $\text{TP}^c\text{-}\mathbb{CTF}_n$ with $n = 3, 4, 5, 6$ in this paper, in particular, for their applications in image processing.

As explained in [23, 24, 25], the directionality of $\text{TP}^b\text{-}\mathbb{CTF}_n$ with $n \geqslant 3$ in high dimensions is mainly because of the following frequency separation property:

$$(2.4) \qquad \widehat{b_\ell^+}(\xi) \approx 0, \quad \xi \in [-\pi, 0] \quad \text{or} \quad \widehat{b_\ell^-}(\xi) \approx 0, \quad \xi \in [0, \pi], \qquad \ell = 1, \ldots, s.$$

That is, all $\widehat{a^+}, \widehat{b_1^+}, \ldots, \widehat{b_s^+}$ nearly vanish on $[-\pi, 0]$ and mostly concentrate on $[0, \pi]$, while all $\widehat{a^-}, \widehat{b_1^-}, \ldots, \widehat{b_s^-}$ nearly vanish on $[0, \pi]$ and mostly concentrate on $[-\pi, 0]$. The frequency

separation property in (2.4) motives the definition of a quantity to measure the frequency separation ability for general filters. In fact, for a filter $b = \{b(k)\}_{k \in \mathbb{Z}}$ which is not identically zero, we introduce the following quantity:

$$(2.5) \qquad \mathrm{fsp}(b) := \frac{\min\left\{\frac{1}{\pi}\int_{-\pi}^{0}|\widehat{b}(\xi)|^2 d\xi, \frac{1}{\pi}\int_{0}^{\pi}|\widehat{b}(\xi)|^2 d\xi\right\}}{\frac{1}{2\pi}\int_{-\pi}^{\pi}|\widehat{b}(\xi)|^2 d\xi}.$$

It is straightforward to observe that $0 \leqslant \mathrm{fsp}(b) \leqslant 1$. The smaller the quantity $\mathrm{fsp}(b)$ is, the better the frequency separation of the filter b will be. If b is a real-valued filter, then $\widehat{b}(\xi) = \overline{\widehat{b}(-\xi)}$ and one can check that $\mathrm{fsp}(b) = 1$. However, things can be quite different for complex-valued filters. Define a sequence $c = \{c(k)\}_{k \in \mathbb{Z}}$ by $\widehat{c}(\xi) := |\widehat{b}(\xi)|^2$ and $C_b := \mathrm{Im}(\sum_{j=1}^{\infty} \frac{c(2j-1)}{2j-1})$, where $\mathrm{Im}(x)$ denotes the imaginary part of $x \in \mathbb{C}$. Noting that $c(k) = \overline{c(-k)}$ for all $k \in \mathbb{Z}$, we have

$$\frac{1}{\pi}\int_{-\pi}^{0}|\widehat{b}(\xi)|^2 d\xi = \frac{1}{\pi}\int_{-\pi}^{0}\widehat{c}(\xi)d\xi = \frac{1}{\pi}\int_{-\pi}^{0}\sum_{k \in \mathbb{Z}}c(k)e^{-ik\xi}d\xi = c(0) + \frac{1}{\pi}\sum_{k \neq 0}\int_{-\pi}^{0}c(k)e^{-ik\xi}d\xi$$

$$= c(0) + \frac{2i}{\pi}\sum_{j \in \mathbb{Z}}\frac{c(2j-1)}{2j-1} = c(0) + \frac{2i}{\pi}\left[\sum_{j=1}^{\infty}\frac{c(2j-1)}{2j-1} + \sum_{j=-\infty}^{0}\frac{c(2j-1)}{2j-1}\right]$$

$$= c(0) + \frac{2i}{\pi}\sum_{j=1}^{\infty}\frac{c(2j-1) - \overline{c(2j-1)}}{2j-1} = c(0) - \frac{4C_b}{\pi}.$$

Similarly, we have $\frac{1}{\pi}\int_{0}^{\pi}|\widehat{b}(\xi)|^2 d\xi = c(0) + \frac{4C_b}{\pi}$. Together with $\frac{1}{2\pi}\int_{-\pi}^{\pi}|\widehat{b}(\xi)|^2 d\xi = c(0) = \|b\|_{l_2(\mathbb{Z})}^2$, the quantity $\mathrm{fsp}(b)$ in (2.5) can be easily computed by

$$\mathrm{fsp}(b) = 1 - \frac{4|C_b|}{\pi c(0)}.$$

For any tight framelet filter bank $\{a; b^+, b^-\}$, i.e., the *perfect reconstruction property* (2.1) holds, with $b^- = \overline{b^+}$, [23, Theorem 1] says

$$(2.6) \qquad \mathrm{fsp}(b^+) = \mathrm{fsp}(b^-) \geqslant \frac{\frac{1}{\pi}\int_{0}^{\pi}A(\xi)d\xi}{1 - \|a\|_{l_2(\mathbb{Z})}^2} =: \mathrm{fslb}_{hp}(a),$$

where hp in $\mathrm{fslb}_{hp}(a)$ stands for high pass and
(2.7)

$$A(\xi) := \frac{2 - |\widehat{a}(\xi)|^2 - |\widehat{a}(\xi+\pi)|^2 - \sqrt{4\big(1 - |\widehat{a}(\xi)|^2 - |\widehat{a}(\xi+\pi)|^2\big) + (|\widehat{a}(\xi)|^2 - |\widehat{a}(\xi+\pi)|^2)^2}}{2}.$$

The quantity $\mathrm{fslb}_{hp}(a)$ in (2.6) gives a lower bound on $\mathrm{fsp}(b^+), \mathrm{fsp}(b^-)$ for the high-pass filters b^+, b^- in a tight framelet filter bank $\{a; b^+, b^-\}$. If the filter a has real coefficients, [23, Theorem 1] further shows that there exists a tight framelet filter bank $\{a; \mathring{b}^+, \mathring{b}^-\}$ with $\mathring{b}^- = \overline{\mathring{b}^+}$

such that $\text{fsp}(\mathring{b}^+) = \text{fsp}(\mathring{b}^-) = \text{fslb}_{hp}(a)$. However, $\mathring{b}^+$ and $\mathring{b}^-$ cannot have finite support in the spatial domain. As shown in [23, Theorem 2], the quantity $\text{fslb}_{hp}(a)$ is often very small for most known low-pass filters in the literature. Though we cannot achieve such a theoretical lower bound when considering compactly supported tight framelet filter banks, in this paper, we can seek compactly supported $\mathbb{CTF}_3$ and $\mathbb{CTF}_4$ with quantities $\text{fsp}(b^\pm)$ as small as possible, which can be done by employing optimization techniques in our design.

3. Splitting low-pass filters with frequency separation property. Two auxiliary filters a^+ and a^- are required in the construction of $\mathbb{CTF}_{2s+2}$ with a positive integer s. Note that the only difference between $\mathbb{CTF}_{2s+1}$ and $\mathbb{CTF}_{2s+2}$ is that we have to split the low-pass filter a in $\mathbb{CTF}_{2s+1}$ into two auxiliary filters a^+ and a^- with a good frequency separation property. In this section, we focus on how to split a real-valued low-pass filter a into two auxiliary filters a^+ and a^- such that $a^- = \overline{a^+}$ with $\widehat{a^+}$ almost vanishing on the interval $[-\pi, 0]$. Then we discuss and introduce a particular family of low-pass filters for our construction of directional compactly supported TP^c-$\mathbb{CTF}_n$ in the next section.

3.1. Analysis and algorithm for splitting a low-pass filter into two auxiliary filters. Given a one-dimensional tight framelet filter bank $\{a; b_1, \ldots, b_s\}$, that is, the perfect reconstruction property (2.1) holds, to preserve the perfect reconstruction property of a new framelet filter bank $\{a^+, a^-; b_1, \ldots, b_s\}$ derived from splitting of a low-pass filter a, the two auxiliary filters a^+ and a^- have to satisfy

$$(3.1) \quad |\widehat{a^+}(\xi)|^2 + |\widehat{a^-}(\xi)|^2 = |\widehat{a}(\xi)|^2 \quad \text{and} \quad \widehat{a^+}(\xi)\overline{\widehat{a^+}(\xi+\pi)} + \widehat{a^-}(\xi)\overline{\widehat{a^-}(\xi+\pi)} = \widehat{a}(\xi)\overline{\widehat{a}(\xi+\pi)}$$

for almost every $\xi \in \mathbb{R}$. The following theorem (see its proof in section 7) provides a theoretical lower bound on how well the frequency separation can be for the two auxiliary filters a^+ and a^- obtained from any splitting of the low-pass filter a satisfying (3.1).

Theorem 3.1. *Let $a \in l_2(\mathbb{Z})$ be a filter on $\mathbb{Z}$. For any complex-valued filters $a^+, a^- \in l_2(\mathbb{Z})$ satisfying (3.1), the following inequality holds:*

$$(3.2) \qquad |\widehat{a^+}(\xi+\pi)|^2 + |\widehat{a^-}(\xi)|^2 \geqslant \min(|\widehat{a}(\xi)|^2, |\widehat{a}(\xi+\pi)|^2), \qquad a.e.\, \xi \in [0, \pi].$$

Moreover, there exist particular filters $a^+, a^- \in l_2(\mathbb{Z})$ satisfying (3.1) and

$$(3.3) \qquad |\widehat{a^+}(\xi+\pi)|^2 + |\widehat{a^-}(\xi)|^2 = \min(|\widehat{a}(\xi)|^2, |\widehat{a}(\xi+\pi)|^2), \qquad a.e.\, \xi \in [0, \pi].$$

If in addition the filter a is real valued, then the particular filters a^+ and a^- can further satisfy the relation $a^- = \overline{a^+}$.

For any two auxiliary filters a^+ and a^- with $a^- = \overline{a^+}$ obtained from splitting a real-valued filter a, according to (3.2) in Theorem 3.1, we must have

$$(3.4) \qquad \text{fsp}(a^+) = \text{fsp}(a^-) \geqslant \frac{\frac{1}{\pi}\int_0^\pi \min(|\widehat{a}(\xi)|^2, |\widehat{a}(\xi+\pi)|^2)d\xi}{\|a\|_{l_2(\mathbb{Z})}^2} =: \text{fslb}_{lp}(a),$$

where lp in $\text{fslb}_{lp}(a)$ stands for low-pass. Note that $0 \leqslant \text{fslb}_{lp}(a) \leqslant 1$. From (3.3), such a lower bound $\text{fslb}_{lp}(a)$ can be achieved by a certain pair (a^+, a^-) of filters, but they are not

finitely supported. Thus, under the setting of compactly supported filters, we instead turn to the searching of pairs (a^+, a^-) with a good frequency separation property.

We study how to split a finitely supported filter a into two finitely supported auxiliary filters a^+ and a^- in the following result whose proof is given in section 7.

Theorem 3.2. *Let $a = \{a(k)\}_{k\in\mathbb{Z}} \in l_0(\mathbb{Z})$ be a finitely supported filter on $\mathbb{Z}$ such that the Laurent polynomials $\mathsf{a}(z)$ and $\mathsf{a}(-z)$ do not have common zeros in $\mathbb{C}\backslash\{0\}$, where $\mathsf{a}(z) := \sum_{k\in\mathbb{Z}} a(k)z^k$. Then (3.1) holds for filters $a^+, a^- \in l_0(\mathbb{Z})$ if and only if there exist $u^+, u^- \in l_0(\mathbb{Z})$ such that*

$$(3.5) \qquad \widehat{a^+}(\xi) = \widehat{a}(\xi)\widehat{u^+}(2\xi), \quad \widehat{a^-}(\xi) = \widehat{a}(\xi)\widehat{u^-}(2\xi) \quad \text{with} \quad |\widehat{u^+}(\xi)|^2 + |\widehat{u^-}(\xi)|^2 = 1.$$

If in addition the filter a is real valued, then both $a^- = \overline{a^+}$ and (3.1) are satisfied if and only if (3.5) holds for some filters $u^+, u^- \in l_0(\mathbb{Z})$ satisfying $u^- = \overline{u^+}$.

Theorem 3.2 makes precise the relation between (a^+, a^-) and a, which essentially says that (a^+, a^-) can be obtained from a via any pair (u^+, u^-) of filters with the *partition of unity property*: $|\widehat{u^+}(\xi)|^2 + |\widehat{u^-}(\xi)|^2 = 1$. For more details, see its proof in section 7. Based on Theorem 3.2 and the frequency separation quantity, we present in Algorithm 3.1 the procedure of splitting a low-pass filter a into two auxiliary filters a^+ and a^- with a good frequency separation property which we summarize here:

(S1) We first parameterize the filters u^+, u^- through u_1 and u_2 as defined in (3.6) with parameters $t_0, \ldots, t_N \in [-\pi, \pi]$ for some N. Since $|\mathsf{u}_1(\xi)|^2 + |\mathsf{u}_2(\xi)|^2 = 1$, it is straightforward to check that $|\widehat{u^+}(\xi)|^2 + |\widehat{u^-}(\xi)|^2 = 1$.

(S2) The two auxiliary filters a^+, a^- are then linked to a through (3.7), which implies that $u^- = \overline{u^+}$.

(S3) This optimization step gives a^+, a^- with small frequency separation quantities $\mathrm{fsp}(a^+)$ and $\mathrm{fsp}(a^-)$. By Theorem 3.2, if the low-pass filter a is real valued, this optimization step is also equivalent to $\min_{t_0,\ldots,t_N} \mathrm{fsp}(a^+)$, and the procedure produces a^+, a^- satisfying $a^- = \overline{a^+}$ and $\mathrm{fsp}(a^-) = \mathrm{fsp}(a^+)$.

3.2. Design and choices of low-pass filters for $\mathbf{TP}^c\text{-}\mathbb{CTF}_n$. With Algorithm 3.1, we know *how* to split a low-pass filter into two auxiliary filters. The question for the construction of compactly supported $\mathbb{CTF}_n$ then becomes *what* kind of low-pass filters we should choose for splitting! This subsection is devoted to answer such a question.

Let us first recall a few quantities for a filter $u \in l_0(\mathbb{Z})$. A filter u has order n of *vanishing moments* if $\widehat{u}(\xi) = \mathcal{O}(|\xi|^n)$ as $\xi \to 0$, and we denote $\mathrm{vm}(u) := n$ with n being the largest such integer. Here we used the notation $\widehat{u}(\xi) = \mathcal{O}(|\xi|^n)$ as $\xi \to 0$ to stand for $\widehat{u}(0) = \widehat{u}'(0) = \cdots = \widehat{u}^{(n-1)}(0) = 0$. A filter u has order m of *sum rules* if $\widehat{u}(\xi + \pi) = \mathcal{O}(|\xi|^m)$ as $\xi \to 0$, and we denote $\mathrm{sr}(u) := m$ with m being the largest such integer. A filter u has order m *linear-phase moments* with phase $c := \mathrm{Re}(\sum_{k\in\mathbb{Z}} u(k)k)$ if $\widehat{u}(\xi) = e^{-ic\xi} + \mathcal{O}(|\xi|^m)$ as $\xi \to 0$ (see [17]). In particular, we denote $\mathrm{lpm}(u) := m$ with m being the largest such integer.

If $\{a; b_1, \ldots, b_s\}$ is a tight framelet filter bank, then it is easy to check ([10] and [22, Proposition 3.3.1]) that

$$(3.8) \qquad \min(\mathrm{vm}(b_1), \ldots, \mathrm{vm}(b_s)) = \min(\mathrm{sr}(a), \tfrac{1}{2}\mathrm{lpm}(a * a^\star)) \quad \text{with} \quad \widehat{a * a^\star}(\xi) := |\widehat{a}(\xi)|^2.$$

Algorithm 3.1 Low-pass filter splitting.

Input: A finitely supported real-valued low-pass filter $a \in l_0(\mathbb{Z})$.

(S1) Choose an integer $N \in \mathbb{N} \cup \{0\}$ and define

$$(3.6) \qquad \begin{bmatrix} \mathsf{u}_1(\xi) & \mathsf{u}_2(\xi) \\ \mathsf{u}_3(\xi) & \mathsf{u}_4(\xi) \end{bmatrix} := \begin{bmatrix} \cos(t_0) & -\sin(t_0) \\ \sin(t_0) & \cos(t_0) \end{bmatrix} \prod_{j=1}^{N} \begin{bmatrix} \cos(t_j) & -\sin(t_j) \\ e^{-i\xi}\sin(t_j) & e^{-i\xi}\cos(t_j) \end{bmatrix},$$

where $t_0, \ldots, t_N \in [-\pi, \pi]$ are real numbers to be determined later.

(S2) Define two filters a^+ and a^- by $\widehat{a^+}(\xi) := \widehat{a}(\xi)\widehat{u^+}(2\xi)$ and $\widehat{a^-}(\xi) := \widehat{a}(\xi)\widehat{u^-}(2\xi)$, where

$$(3.7) \qquad \widehat{u^+}(\xi) := [\mathsf{u}_1(\xi) + i\mathsf{u}_2(\xi)]/\sqrt{2}, \qquad \widehat{u^-}(\xi) := [\mathsf{u}_1(\xi) - i\mathsf{u}_2(\xi)]/\sqrt{2}.$$

(S3) Find a solution $\{t_0, \ldots, t_N\}$ of the following optimization problem:

$$\min_{t_0,\ldots,t_N} \int_0^\pi \left(|\widehat{a^+}(\xi + \pi)|^2 + |\widehat{a^-}(\xi)|^2 \right) d\xi.$$

Ouput: Filters a^+ and a^- satisfying all the conditions in (3.1) with $a^- = \overline{a^+}$.

In order to have high vanishing moments for the high-pass filters $b_1, \ldots, b_s$, it is necessary for the low-pass filter a to have large sum rules $\mathrm{sr}(a)$ and high linear-phase moments $\mathrm{lpm}(a * a^\star)$.

In the context of filter design, there are a few statistics-related quantities that are of interest in applications. Following [22, (2.0.8) and (2.0.9)], for a filter $u = \{u(k)\}_{k\in\mathbb{Z}} \in l_0(\mathbb{Z})$, we define its expectation/mean $\mathrm{E}(u)$ and (normalized) variance $\mathrm{Var}(u)$ by

$$\mathrm{E}(u) := \frac{\sum_{k\in\mathbb{Z}} |u(k)|^2 k}{\|u\|_{l_2(\mathbb{Z})}^2} \qquad \text{and} \qquad \mathrm{Var}(u) := \frac{\sum_{k\in\mathbb{Z}} |u(k)|^2 (k - \mathrm{E}(u))^2}{\|u\|_{l_2(\mathbb{Z})}^2}.$$

Note that $\mathrm{Var}(u) = \min_{c\in\mathbb{R}} \sum_{k\in\mathbb{Z}} |u(k)|^2 (k - c)^2 / \|u\|_{l_2(\mathbb{Z})}^2$ with the minimum value achieved at $c = \mathrm{E}(u)$. The smaller the quantity $\mathrm{Var}(u)$, the better spatial localization of the filter u.

To build directional compactly supported $\mathrm{TP}^c\text{-}\mathbb{C}\mathrm{TF}_n$, we have to design one-dimensional complex tight framelet filter banks $\mathbb{C}\mathrm{TF}_n$ from a given low-pass filter a:

$$\mathbb{C}\mathrm{TF}_n = \begin{cases} \{a; b_1^+, \ldots, b_s^+, b_1^-, \ldots, b_s^-\} & \text{if } n = 2s + 1 \text{ is odd,} \\ \{a^+, a^-; b_1^+, \ldots, b_s^+, b_1^-, \ldots, b_s^-\} & \text{if } n = 2s + 2 \text{ is even.} \end{cases}$$

The following are some desirable properties for a low-pass filter a in a $\mathbb{C}\mathrm{TF}_n$:

(i) relatively large sum rules $\mathrm{sr}(a)$ and high linear-phase moments $\mathrm{lpm}(a * a^\star)$;

(ii) small frequency separation quantities $\mathrm{fslb}_{hp}(a)$ and $\mathrm{fslb}_{lp}(a)$ as in (2.6) and (3.4), respectively;

(iii) small variance $\mathrm{Var}(a)$ and short support length $\mathrm{len}(a)$.

By the identity in (3.8), item (i) guarantees that all the high-pass filters $b_1^+, \ldots, b_s^+$, $b_1^-, \ldots, b_s^-$ in the tight framelet filter bank $\mathbb{C}\mathrm{TF}_n$ have a relatively high order of vanishing moments, which are closely related to the sparse representation of their associated tight

Table 1

The frequency separation quantities $\mathrm{fslb}_{hp}(a)$ and $\mathrm{fslb}_{lp}(a)$ for three low-pass filter families: the B-spline filters a_m^B, the interpolatory filters a_m^I, and the Daubechies orthogonal wavelet filters a_m^D for $m = 1, \ldots, 8$. Note that for Daubechies orthogonal wavelet filters, we have $\mathrm{fslb}_{lp}(a_m^D) = \mathrm{fslb}_{hp}(a_m^D)$. The listed variance $\mathrm{Var}(a_m^D)$ is the smallest among all possible choices of a_m^D satisfying $|\widehat{a_m^D}(\xi)|^2 = \widehat{a_{2m}^I}(\xi)$.

m	1	2	3	4	5	6	7	8
$\mathrm{Var}(a_m^B)$	0.250000	0.333333	0.450000	0.571429	0.694444	0.818182	0.942308	1.06667
$\mathrm{Var}(a_{2m}^I)$	0.333333	0.428571	0.507137	0.574308	0.633798	0.687718	0.737374	0.783634
$\mathrm{Var}(a_m^D)$	0.250000	0.328124	0.453684	0.425360	0.559572	0.531640	0.569226	0.631786
$\mathrm{fslb}_{lp}(a_m^B)$	0.363380	0.151173	0.066291	0.029913	0.013745	0.006395	0.003004	0.001421
$\mathrm{fslb}_{lp}(a_{2m}^I)$	0.151173	0.094585	0.073303	0.061623	0.054049	0.048651	0.044564	0.041335
$\mathrm{fslb}_{lp}(a_m^D)$	0.363380	0.257277	0.209530	0.181110	0.161768	0.147526	0.136479	0.127588
$\mathrm{fslb}_{hp}(a_m^B)$	0.363380	0.027195	0.004327	0.000822	0.000170	0.000037	0.000008	0.000002
$\mathrm{fslb}_{hp}(a_{2m}^I)$	0.027195	0.020072	0.016720	0.014666	0.013237	0.012168	0.011328	0.010645
$\mathrm{fslb}_{hp}(a_m^D)$	0.363380	0.257277	0.209530	0.181110	0.161768	0.147526	0.136479	0.127588

framelets. Moreover, large $\mathrm{lpm}(a * a^\star)$ implies that $|\widehat{a}(\xi)|^2$ is very close to 1 in a neighborhood of the origin. If $1 - |\widehat{a}(\xi)|^2$ is not very small in a neighborhood of the origin, then the low frequency information of a transformed signal will significantly leak away for the high-pass filters to handle and will result in a not-so-good frequency balance between the low-pass filter and high-pass filters. Due to (2.6) and (3.4), item (ii) is important for the auxiliary filters a^+, a^- and all the high-pass filters $b_1^+, \ldots, b_s^+, b_1^-, \ldots, b_s^-$ to have good frequency separation properties simultaneously. Small $\mathrm{Var}(a)$ in item (iii) means good spatial localization of the low-pass filter a and short support length $\mathrm{len}(a)$ improves computational efficiency. More importantly, larger $\mathrm{len}(a)$ means longer support of a and all its derived high-pass filters often have longer support as well. This not only worsens the computational efficiency but also makes the construction of one-dimensional complex tight framelet filter bank $\mathbb{CTF}_n$ much more complicated.

We now examine three popular filter families in literature:

(1) The *B-spline filter* a_m^B of order m is given by $\widehat{a_m^B}(\xi) := 2^{-m}(1 + e^{-i\xi})^m$, $m \in \mathbb{N}$.

(2) The *interpolatory filter* a_{2m}^I is given by $\widehat{a_{2m}^I}(\xi) := \cos^{2m}(\xi/2)\mathsf{P}_{m,m}(\sin^2(\xi/2))$, where

$$(3.9) \qquad \mathsf{P}_{m,\ell}(x) := \sum_{j=0}^{\ell-1} \binom{m+j-1}{j} x^j.$$

(3) The *Daubechies orthogonal wavelet low-pass filter* a_m^D of order m is supported on $[0, 2m-1]$ and satisfies $|\widehat{a_m^D}(\xi)|^2 = \widehat{a_{2m}^I}(\xi) := \cos^{2m}(\xi/2)\mathsf{P}_{m,m}(\sin^2(\xi/2))$.

We refer to [6, 9] and [22, sections 2.1–2.2] for more details about these families of filters. The variance $\mathrm{Var}(a)$ and the frequency separation quantities $\mathrm{fslb}_{lp}(a)$ and $\mathrm{fslb}_{hp}(a)$ are listed in Table 1 for these three filter families.

Table 1 indicates that B-spline filters have small frequency separation quantities $\mathrm{fslb}_{hp}(a_m^B)$ and $\mathrm{fslb}_{lp}(a_m^B)$ with high sum rules $\mathrm{sr}(a_m^B) = m$ and very short support $\mathrm{len}(a_m^B) = m$. However, a_m^B has relatively large variance (and, hence, is not that good in spatial localization) and very low linear-phase moments with $\mathrm{lpm}(a_m^B * (a_m^B)^\star) = 2$, which forces all the high-pass filters in any

constructed tight framelet filter bank $\mathbb{CTF}_n$ to have at most one vanishing moment. In fact, the function $1 - |\widehat{a_m^B}(\xi)|^2$ is not that small in a neighborhood of the origin and, consequently, a significant portion of the low frequency information will leak away to be handled by the high-pass filters. This requires their associated high-pass filters to be extremely efficient for reasonably good performance in applications, which prevents B-spline filters a_m^B from being effective for our construction of compactly supported $\mathbb{CTF}_n$.

From Table 1, we see that the interpolatory filter a_{2m}^I has small frequency separation quantities $\mathrm{fslb}_{hp}(a_{2m}^I)$ and $\mathrm{fslb}_{lp}(a_{2m}^I)$ with high sum rules $\mathrm{sr}(a_{2m}^I) = 2m$ and reasonably small variance $\mathrm{Var}(a_{2m}^I)$. Therefore, the family of interpolatory filters a_{2m}^I is a good choice as the low-pass filters for our purpose. Though a_{2m}^I filters have symmetry, the filter support of a_{2m}^I is twice as long as that of a_m^D and, consequently, the high-pass filters derived from a_{2m}^I tend to have very long support.

We say that $a \in l_0(\mathbb{Z})$ is *an orthogonal wavelet low-pass filter* if $|\widehat{a}(\xi)|^2 + |\widehat{a}(\xi + \pi)|^2 = 1$. For an orthogonal wavelet low-pass filter a, by [23, Theorem 2], we have $A(\xi) = \min(|\widehat{a}(\xi)|^2, |\widehat{a}(\xi+\pi)|^2)$, where A is defined in (2.7). Therefore, we can verify that $\mathrm{fslb}_{hp}(a) = \mathrm{fslb}_{lp}(a)$ and $\|a\|_{l_2(\mathbb{Z})}^2 = 1/2$. From Table 1, we see that the family of Daubechies orthogonal wavelet filters a_m^D has reasonably small variance $\mathrm{Var}(a_m^D)$ with very short support $\mathrm{len}(a_m^D) = m$. However, the frequency separation quantity $\mathrm{fslb}_{hp}(a_m^D)$ is not that small and decreases slowly at the expense of longer filter supports. In addition, since $A(\xi) = \min(|\widehat{a_m^D}(\xi)|^2, |\widehat{a_m^D}(\xi + \pi)|^2)$ and $|\widehat{a_m^D}(\xi)|^2 + |\widehat{a_m^D}(\xi + \pi)|^2 = 1$, we see that

$$A(\pi/2) = |\widehat{a_m^D}(\pi/2)|^2 = 1/2,$$

which is independent of the choice of m. This creates a fixed peak point for the function A and forces that the frequency separation of all its derived high-pass filters cannot be that good.

By sacrificing symmetry of a low-pass filter to achieve short support, we now construct a particular family of low-pass filters by combining the advantages of both interpolatory and orthogonal wavelet filters for directional compactly supported TP^c-$\mathbb{CTF}_n$.

To construct one-dimensional tight framelet filter banks $\mathbb{CTF}_n$, we have to first construct a real-valued low-pass filter $a \in l_0(\mathbb{Z})$ satisfying $\widehat{a}(0) = 1$ and the following necessary condition

$$(3.10) \qquad\qquad |\widehat{a}(\xi)|^2 + |\widehat{a}(\xi + \pi)|^2 \leqslant 1 \qquad \forall \xi \in \mathbb{R}.$$

Then there exist a nonnegative integer m and a polynomial P with real coefficients such that

$$(3.11) \qquad\qquad |\widehat{a}(\xi)|^2 = \cos^{2m}(\xi)\mathsf{P}(\sin^2(\xi/2)),$$

and P satisfies

$$(3.12) \qquad \mathsf{P}(0) = 1, \quad \mathsf{P}(x) \geqslant 0, \quad \text{and} \quad (1-x)^m \mathsf{P}(x) + x^m \mathsf{P}(1-x) \leqslant 1 \qquad \forall\, x \in [0,1].$$

Conversely, if a polynomial P has real coefficients and satisfies (3.12), by the Fejér–Riesz lemma, we can construct a filter $a \in l_0(\mathbb{Z})$ such that $\widehat{a}(0) = 1$ and (3.11) holds.

The following theorem (see section 7 for its proof) provides a family of polynomials P for (3.11) so that one can choose appropriate parameters to balance the requirement among sum rules, linear-phase moments, frequency separation, short supports, etc.

Theorem 3.3. *Let $\ell, m \in \mathbb{N}$ with $1 \leqslant \ell \leqslant m$ and $\frac{1}{2} < c \leqslant 1$. Define a polynomial*

$$(3.13) \qquad\qquad \mathsf{P}(x) := \mathsf{P}_{m,\ell}(x) + x^\ell \left(c_0 - (c_1 + 2c_0)x \right),$$

where $c_0, c_1 \in \mathbb{R}$ and $\mathsf{P}_{m,\ell}$ is defined in (3.9). *If one chooses*

$$(3.14) \quad c_0 = \frac{c\mathsf{P}'_{m,\ell}(c) - (\ell+1)\mathsf{P}_{m,\ell}(c)}{c^\ell} \quad and \quad c_1 = \frac{(1-2c)\mathsf{P}'_{m,\ell}(c) + (2 + 2\ell - \ell/c)\mathsf{P}_{m,\ell}(c)}{c^\ell},$$

then $c_0 < 0$, $c_1 > 0$, and (3.12) *holds. Therefore, there is a finitely supported low-pass filter $a \in l_0(\mathbb{Z})$ satisfying* (3.11) *with $\widehat{a}(0) = 1$, $\mathrm{sr}(a) = m$, and $\mathrm{lpm}(a * a^\star) = 2\ell$.*

The parameters c_0 and c_1 are used to add a double root at the point c for the polynomial P defined in (3.13) so that the frequency response of $\widehat{a}$ derived from P is dumped near the point $2\arcsin\sqrt{c} \in [0, \pi]$ with small frequency separation quantities $\mathrm{fslb}_{hp}(a)$ and $\mathrm{fslb}_{lp}(a)$. In applications, we often choose $c = 1$ and $\ell \in \{m-1, m\}$.

4. Construction of directional compactly supported tensor product complex tight framelets. In this section we provide algorithms for the construction of directional compactly supported $\mathrm{TP}^c\text{-}\mathbb{CTF}_n$ with $n = 3, 4, 5, 6$, and present several concrete examples to illustrate our proposed algorithms.

4.1. Algorithms for compactly supported complex tight framelets $\mathbb{CTF}_n$. We first discuss how to construct directional compactly supported $\mathrm{TP}^c\text{-}\mathbb{CTF}_3$ and $\mathrm{TP}^c\text{-}\mathbb{CTF}_4$ by constructing compactly supported one-dimensional filter banks $\mathbb{CTF}_3$ and $\mathbb{CTF}_4$. We observe that the key and only difference between $\mathbb{CTF}_3$ and $\mathbb{CTF}_4$ lies in that we have to split the low-pass filter a into two auxiliary filters a^+ and a^- with frequency separation for $\mathbb{CTF}_4$. By modifying [23, Algorithm 2], we present in Algorithm 4.1 the construction of $\mathbb{CTF}_3 = \{a; b^+, b^-\}$ and $\mathbb{CTF}_4 = \{a^+, a^-; b^+, b^-\}$ which we summarize here:

- (S1) Split a suitable low-pass filter a to two auxiliary filters a^+, a^- using Algorithm 3.1.
- (S2) Construct a tight framelet filter bank $\{a; b_1, b_2\}$ from a (see, e.g., [20, 21, 23]).
- (S3) Parameterize v_1, v_2 through $\mathsf{u}_1, \mathsf{u}_2, \mathsf{u}_3, \mathsf{u}_4$ as in (3.6). Note that $|\widehat{v_1}(\xi)|^2 + |\widehat{v_2}(\xi)|^2 = 1$.
- (S4) The filters b^+, b^- are linked to b_1, b_2 through (4.1). One can easily show that such b^+, b^- preserve the perfect reconstruction property of $\{a; b^+, b^-\}$.
- (S5) This optimization step gives compactly supported $\mathbb{CTF}_3$ and $\mathbb{CTF}_4$ with small frequency separation quantities $\mathrm{fsp}(a^+)$ and $\mathrm{fsp}(b^+)$.

Similarly to $\mathrm{TP}^c\text{-}\mathbb{CTF}_3$ and $\mathrm{TP}^c\text{-}\mathbb{CTF}_4$, we construct one-dimensional compactly supported filter banks $\mathbb{CTF}_5$ and $\mathbb{CTF}_6$ for $\mathrm{TP}^c\text{-}\mathbb{CTF}_5$ and $\mathrm{TP}^c\text{-}\mathbb{CTF}_6$, respectively. The only difference between $\mathbb{CTF}_5$ and $\mathbb{CTF}_6$ again lies in that we have to split the low-pass filter a into two auxiliary filters a^+ and a^- for $\mathbb{CTF}_6$ by Algorithm 3.1. Instead of parameterizing 2π-periodic trigonometric polynomials, we directly employ optimization techniques to minimize the frequency separation quantities. We present in Algorithm 4.2 the construction of $\mathbb{CTF}_5 = \{a; b_1^+, b_2^+, b_1^-, b_2^-\}$ and $\mathbb{CTF}_6 = \{a^+, a^-; b_1^+, b_2^+, b_1^-, b_2^-\}$ which we summarize here:

- (S1) Construct two auxiliary filters a^+, a^- from a using Algorithm 3.1.
- (S2) Directly parameterize $b_1^+, b_1^-, b_2^+, b_2^-$ through (4.2).
- (S3) This optimization step gives compactly supported $\mathbb{CTF}_5$ and $\mathbb{CTF}_6$ with desired frequency separation quantities $\mathrm{fsp}(a^+)$, $\mathrm{fsp}(b_1^+)$, and $\mathrm{fsp}(b_2^+)$.

Algorithm 4.1 Construction of compactly supported $\mathbb{CTF}_3$ and $\mathbb{CTF}_4$.

Input: A real-valued filter $a \in l_0(\mathbb{Z})$ satisfying $|\widehat{a}(\xi)|^2 + |\widehat{a}(\xi + \pi)|^2 \leqslant 1$ for all $\xi \in \mathbb{R}$.

(S1) Construct two filters a^+ and a^- with $a^- = \overline{a^+}$ from the filter a by Algorithm 3.1 with small $\mathrm{fsp}(a^+)$.

(S2) Construct a finitely supported real-valued tight framelet filter bank $\{a; b_1, b_2\}$ from the filter a by [21, Algorithm 4].

(S3) Choose a suitable integer $N \in \mathbb{N} \cup \{0\}$ and define 2π-periodic trigonometric polynomials $\mathsf{u}_1, \mathsf{u}_2, \mathsf{u}_3, \mathsf{u}_4$ as in (3.6), where $t_0, \dots, t_N \in [-\pi, \pi]$ are real numbers to be determined later.

(S4) Define two high-pass filters b^+ and b^- by

$$(4.1) \qquad \widehat{b^+}(\xi) := \widehat{b_1}(\xi)\widehat{v_1}(2\xi) + \widehat{b_2}(\xi)\widehat{v_2}(2\xi), \qquad b^- := \overline{b^+},$$

with

$$\widehat{v_1}(\xi) := [\mathsf{u}_1(\xi) + i\mathsf{u}_2(\xi)]/\sqrt{2}, \qquad \widehat{v_2}(\xi) := [\mathsf{u}_3(\xi) + i\mathsf{u}_4(\xi)]/\sqrt{2}.$$

(S5) Find a solution $\{t_0, \dots, t_N\}$ to the following optimization problem:

$$\min_{t_0, \dots, t_N} \int_0^\pi |\widehat{b^+}(\xi + \pi)|^2 d\xi,$$

which is equivalent to the optimization problem: $\min_{t_0, \dots, t_N} \mathrm{fsp}(b^+)$.

Ouput: Tight framelet filter banks $\mathbb{CTF}_3 := \{a; b^+, b^-\}$ and $\mathbb{CTF}_4 := \{a^+, a^-; b^+, b^-\}$.

We make some remarks here about Algorithms 4.1 and 4.2.

(1) The simple splitting technique in Algorithm 4.1 is generally not that easy to generalize to construct $\mathbb{CTF}_5$ and $\mathbb{CTF}_6$. This is largely due to the lack of a similar result as in [23, Theorem 3.1] for linking all tight framelet filter banks with four high-pass filters, and the parameterization of all 4×4 paraunitary matrices is unknown without involving complicated structures.

(2) At the cost of losing simplicity and completeness, the direct method using optimization in Algorithm 4.2 appears to work well in general. To achieve directionality for $\mathbb{CTF}_5$ and $\mathbb{CTF}_6$, the filter $\widehat{b_1^+}$ should largely concentrate on the middle frequency band of $[0, \pi]$ and $\widehat{b_2^+}$ should largely concentrate on the high frequency band of $[0, \pi]$. This goal is roughly achieved in Algorithm 4.2 through minimizing the quantity in (4.3) with the heuristically chosen intervals and regularization parameters $\lambda_1, \dots, \lambda_4$ in step (S3) of Algorithm 4.2. Heuristically, Algorithm 4.2 forces that $\widehat{b_1^+}$ mostly concentrates on the middle frequency band/interval $[\frac{\pi}{4}, \frac{7\pi}{12}]$ and almost vanishes on $[-\frac{\pi}{2}, 0]$, while $\widehat{b_2^+}$ mostly concentrates on the high frequency band/interval $[\frac{\pi}{2}, \frac{5\pi}{6}]$ and almost vanishes on $[-\frac{3\pi}{4}, -\frac{5\pi}{12}]$.

(3) The optimization problem in Algorithm 4.2 for directionality of the two high-pass filters is much more complicated than Algorithm 3.1 or 4.1 for just one high-pass filter. The minimization problems in Algorithms 3.1 and 4.1 are both quadratic program

---

Algorithm 4.2 Construction of compactly supported $\mathbb{CTF}_5$ and $\mathbb{CTF}_6$.

Input: A real-valued filter $a \in l_0(\mathbb{Z})$ satisfying $|\widehat{a}(\xi)|^2 + |\widehat{a}(\xi + \pi)|^2 \leqslant 1$ for all $\xi \in \mathbb{R}$.

(S1) Construct two filters a^+ and a^- with $a^- = \overline{a^+}$ from the filter a by Algorithm 3.1 with small $\mathrm{fsp}(a^+)$.

(S2) Choose a suitable integer $N \in \mathbb{N} \cup \{0\}$ and parameterize high-pass filters b_1^+, b_1^- and b_2^+, b_2^- with $b_1^- := \overline{b_1^+}$ and $b_2^- := \overline{b_2^+}$ by

$$(4.2) \quad \widehat{b_1^+}(\xi) := t_0 + t_1 e^{-i\xi} + \cdots + t_N e^{-iN\xi}, \quad \widehat{b_2^+}(\xi) := c_0 + c_1 e^{-i\xi} + \cdots + c_N e^{-iN\xi},$$

where $t_0, \ldots, t_N, c_0, \ldots, c_N$ are complex numbers to be determined later.

(S3) Find a solution $\{t_0, \ldots, t_N, c_0, \ldots, c_N\}$ of complex numbers to the following constrained optimization problem:
$$(4.3)$$
$$\min_{\substack{t_k, c_k, \\ k=0,\ldots,N}} -\lambda_1 E_1\left(\left[\tfrac{\pi}{4}, \tfrac{7\pi}{12}\right]\right) - \lambda_2 E_2\left(\left[\tfrac{\pi}{2}, \tfrac{5\pi}{6}\right]\right) + \lambda_3 E_1\left(\left[-\tfrac{\pi}{2}, 0\right]\right) + \lambda_4 E_2\left(\left[-\tfrac{3\pi}{4}, -\tfrac{5\pi}{12}\right]\right),$$

where $\lambda_1, \ldots, \lambda_4$ are real positive regularization parameters and

$$E_j([\alpha, \beta]) := \int_\alpha^\beta |\widehat{b_j^+}(\xi)|^2 d\xi, \quad -\pi \leqslant \alpha < \beta \leqslant \pi, \; j = 1, 2,$$

under the constraints for a tight framelet filter bank $\{a; b_1^+, b_2^+, b_1^-, b_2^-\}$:

$$\begin{cases} |\widehat{b_1^+}(\xi)|^2 + |\widehat{b_2^+}(\xi)|^2 + |\widehat{b_1^-}(\xi)|^2 + |\widehat{b_2^-}(\xi)|^2 & = 1 - |\widehat{a}(\xi)|^2, \\[2mm] \sum_{\ell=1}^2 \left(\widehat{b_\ell^+}(\xi)\overline{\widehat{b_\ell^+}(\xi + \pi)} + \widehat{b_\ell^-}(\xi)\overline{\widehat{b_\ell^-}(\xi + \pi)} \right) & = -\widehat{a}(\xi)\overline{\widehat{a}(\xi + \pi)}, \end{cases}$$

for all $\xi \in \mathbb{R}$ (such constraints on b_1^+, b_2^+, b_1^-, and b_2^- can be rewritten as equations in terms of $t_0, \ldots, t_N, c_0, \ldots, c_N$).

Ouput: Filter banks $\mathbb{CTF}_5 := \{a; b_1^+, b_2^+, b_1^-, b_2^-\}$ and $\mathbb{CTF}_6 := \{a^+, a^-; b_1^+, b_2^+, b_1^-, b_2^-\}$.

---

problems without any constraint, which can be solved using an iterative active-set method (we use the numerical routine *Minimize* in the numerical algebra software MAPLE). The optimization problem in Algorithm 4.2 minimizes a quadratic objective function with quadratic constraints, which is a nonlinear optimization problem (MAPLE routine *NLPSolve* is used) and one can only expect local minimal solutions.

4.2. Examples of compactly supported $\mathbb{CTF}_n$ with $n = 3, 4, 5, 6$. To illustrate Algorithms 4.1 and 4.2, we now present several concrete examples. In all these examples, optimization routines in MAPLE are used as discussed above and we set the regularization parameters $\lambda_1 = 2.2$, $\lambda_2 = 1$, $\lambda_3 = 0$, and $\lambda_4 = 2.5$ for Algorithm 4.2. We remark that all filters in these examples are available in the MATLAB package `cptTPCTF` that can be found in http://staffweb1.cityu.edu.hk/xzhuang7.

Example 1. Taking $m = 2$ from the family of interpolatory filters a_{2m}^I as the low-pass filter a,

$$a = a_4^I = \left\{ -\tfrac{1}{32}, 0, \tfrac{9}{32}, \tfrac{1}{2}, \tfrac{9}{32}, 0, -\tfrac{1}{32} \right\}_{[-3,3]}.$$

Then by calculation we have $\mathrm{sr}(a) = 4$, $\mathrm{lpm}(a * a^\star) = 4$, and

$$\|a\|_{l_2(\mathbb{Z})} = \tfrac{\sqrt{105}}{16}, \quad \mathrm{fslb}_{hp}(a) \approx 0.02007, \quad \text{and} \quad \mathrm{fslb}_{lp}(a) \approx 0.09459.$$

Applying Algorithm 3.1 with $N = 2$ to split the low-pass filter a, we obtain two auxiliary filters a^+ and a^- with $a^- = \overline{a^+}$ and

$$
\begin{aligned}
a^+ = \{ &(-1.575\mathrm{E}{-}2), (0), (1.428\mathrm{E}{-}1) + (1.542\mathrm{E}{-}2)\,i, (2.519\mathrm{E}{-}1), (1.316\mathrm{E}{-}1) - (1.377\mathrm{E}{-}1)\,i, \\
&(-1.790\mathrm{E}{-}2) - (2.467\mathrm{E}{-}1)\,i, (-2.581\mathrm{E}{-}2) - (1.491\mathrm{E}{-}1)\,i, -(1.828\mathrm{E}{-}2)\,i, \\
&(1.119\mathrm{E}{-}3) + (5.140\mathrm{E}{-}3)\,i, (0), (1.142\mathrm{E}{-}3)\,i \}_{[-3,7]}.
\end{aligned}
$$

Then $\mathrm{fsp}(a^+) = \mathrm{fsp}(a^-) \approx 0.3727$, $\|a^+\|_{l_2(\mathbb{Z})} = \|a^-\|_{l_2(\mathbb{Z})} \approx 0.4529$.

This low-pass filter a has already been used to construct compactly supported $\mathbb{CTF}_3$ in [23, Example 3]. By [21, Algorithm 4], we have a real-valued initial tight framelet filter bank $\{a; b_1, b_2\}$ with

$$b_1 = \{-3.6038\mathrm{E}{-}3, 0, 5.6537\mathrm{E}{-}2, 5.7661\mathrm{E}{-}2, 4.0675\mathrm{E}{-}3, -3.8564\mathrm{E}{-}1, 2.7098\mathrm{E}{-}1\}_{[-3,3]},$$
$$b_2 = \{4.5667\mathrm{E}{-}3, 0, -1.2476\mathrm{E}{-}1, -7.3067\mathrm{E}{-}2, 4.9759\mathrm{E}{-}1, -3.0433\mathrm{E}{-}1\}_{[-3,2]}.$$

Applying Algorithm 4.1 with $N = 2$, we obtain high-pass filters b^+ and b^- with $b^- = \overline{b^+}$ and

$$
\begin{aligned}
b^+ = \{ &(1.278\mathrm{E}{-}4) + (4.686\mathrm{E}{-}4)\,i, (0), (-3.068\mathrm{E}{-}3) - (1.570\mathrm{E}{-}2)\,i, (-2.045\mathrm{E}{-}3) - (7.497\mathrm{E}{-}3)\,i, \\
&(-3.741\mathrm{E}{-}2) + (4.811\mathrm{E}{-}2)\,i, (-6.660\mathrm{E}{-}2) - (1.729\mathrm{E}{-}1)\,i, (3.502\mathrm{E}{-}1) + (1.316\mathrm{E}{-}1)\,i, \\
&(-2.453\mathrm{E}{-}1) + (1.696\mathrm{E}{-}1)\,i, (-1.514\mathrm{E}{-}2) - (1.484\mathrm{E}{-}1)\,i, (-3.957\mathrm{E}{-}2) + (1.079\mathrm{E}{-}2)\,i, \\
&(5.882\mathrm{E}{-}2) - (1.604\mathrm{E}{-}2)\,i \}_{[-5,5]},
\end{aligned}
$$

which is the same as [23, Example 3]. Then $\mathbb{CTF}_3 = \{a; b^+, b^-\}$ and $\mathbb{CTF}_4 = \{a^+, a^-; b^+, b^-\}$ are tight framelet filter banks with

$$\mathrm{fsp}(b^+) = \mathrm{fsp}(b^-) \approx 0.1658, \quad \mathrm{vm}(b^+) = \mathrm{vm}(b^-) = 2, \quad \|b^+\|_{l_2(\mathbb{Z})} = \|b^-\|_{l_2(\mathbb{Z})} \approx 0.5431.$$

Applying Algorithm 4.2 with $N = 4$, we obtain filters b_1^+, b_2^+, b_1^-, and b_2^- with $b_1^- := \overline{b_1^+}$ and $b_2^- := \overline{b_2^+}$, where

$$
\begin{aligned}
b_1^+ = \{ &(-2.721\mathrm{E}{-}2) + (1.542\mathrm{E}{-}2)\,i, (4.983\mathrm{E}{-}2) - (8.944\mathrm{E}{-}3)\,i, (-2.428\mathrm{E}{-}2) - (3.058\mathrm{E}{-}2)\,i, \\
&(-3.974\mathrm{E}{-}2) + (6.901\mathrm{E}{-}2)\,i, (7.138\mathrm{E}{-}2) + (5.304\mathrm{E}{-}2)\,i, (9.093\mathrm{E}{-}2) - (1.299\mathrm{E}{-}1)\,i, \\
&(-7.919\mathrm{E}{-}2) - (7.760\mathrm{E}{-}2)\,i, (-1.433\mathrm{E}{-}1) + (5.829\mathrm{E}{-}2)\,i, (5.164\mathrm{E}{-}2) + (9.175\mathrm{E}{-}2)\,i, \\
&(5.313\mathrm{E}{-}2) - (3.479\mathrm{E}{-}2)\,i, (0), (-3.228\mathrm{E}{-}3) - (5.735\mathrm{E}{-}3)\,i \}_{[-4,7]}, \\
b_2^+ = \{ &(7.401\mathrm{E}{-}2) - (3.103\mathrm{E}{-}2)\,i, (-1.736\mathrm{E}{-}1) + (1.766\mathrm{E}{-}2)\,i, (1.818\mathrm{E}{-}1) + (1.158\mathrm{E}{-}1)\,i, \\
&(-9.568\mathrm{E}{-}2) - (2.261\mathrm{E}{-}1)\,i, (-3.653\mathrm{E}{-}2) + (1.838\mathrm{E}{-}1)\,i, (9.591\mathrm{E}{-}2) - (7.370\mathrm{E}{-}2)\,i, \\
&(-4.408\mathrm{E}{-}2) - (6.413\mathrm{E}{-}3)\,i, (-2.975\mathrm{E}{-}2) + (2.109\mathrm{E}{-}2)\,i, (1.338\mathrm{E}{-}2) + (3.223\mathrm{E}{-}2)\,i, \\
&(1.539\mathrm{E}{-}2) - (3.142\mathrm{E}{-}2)\,i, (0), (-8.361\mathrm{E}{-}4) - (2.014\mathrm{E}{-}3)\,i \}_{[-4,7]}.
\end{aligned}
$$

(a) $|\widehat{a}|$ and $|\widehat{a^+}|$ (b) $|\widehat{b^+}|$ (c) $|\widehat{b_1^+}|$ and $|\widehat{b_2^+}|$
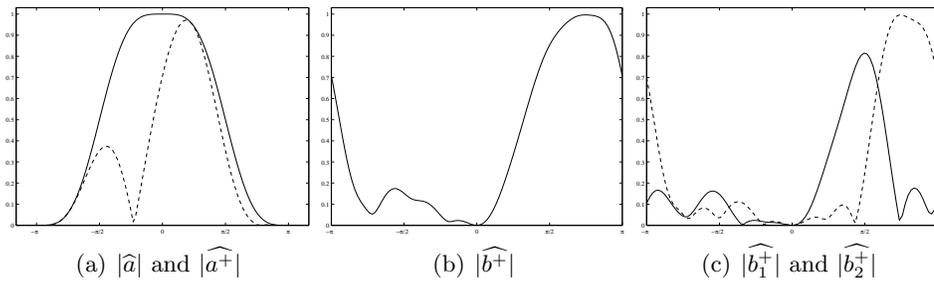
Figure 4. *The frequency separation properties of filters in Example* 1 *on the basic interval* $[-\pi, \pi]$: (a) $|\widehat{a}|$ *(solid line) and* $|\widehat{a^+}|$ *(dashed line).* (b) $|\widehat{b^+}|$. (c) $|\widehat{b_1^+}|$ *(solid line) and* $|\widehat{b_2^+}|$ *(dashed line).*

Then $\mathbb{CTF}_5 = \{a; b_1^+, b_2^+, b_1^-, b_2^-\}$ and $\mathbb{CTF}_6 = \{a^+, a^-; b_1^+, b_2^+, b_1^-, b_2^-\}$ are tight framelet filter banks with

$$\mathrm{fsp}(b_1^+) = \mathrm{fsp}(b_1^-) \approx 0.09119, \quad \mathrm{vm}(b_1^+) = \mathrm{vm}(b_1^-) = 2, \quad \|b_1^+\|_{l_2(\mathbb{Z})} = \|b_1^-\|_{l_2(\mathbb{Z})} \approx 0.3096,$$
$$\mathrm{fsp}(b_2^+) = \mathrm{fsp}(b_2^-) \approx 0.1610, \quad \mathrm{vm}(b_2^+) = \mathrm{vm}(b_2^-) = 2, \quad \|b_2^+\|_{l_2(\mathbb{Z})} = \|b_2^-\|_{l_2(\mathbb{Z})} \approx 0.4462.$$

See Figure 4 for the graphs of the frequency separation properties of a^+, b^+, b_1^+, and b_2^+.

Example 2. Taking $\ell = m = 3$ and $c = 1$ in Theorem 3.3, we obtain a low-pass filter a as follows:

$$a = \Big\{ -\frac{\sqrt{7+2\sqrt{21}}}{128} + \frac{1+\sqrt{21}}{128}, -\frac{5\sqrt{7+2\sqrt{21}}}{128} + \frac{3\sqrt{21}+7}{128}, -\frac{9\sqrt{7+2\sqrt{21}}}{128} + \frac{21+\sqrt{21}}{128}, \frac{35-5\sqrt{21}}{128} - \frac{5\sqrt{7+2\sqrt{21}}}{128},$$
$$\frac{35-5\sqrt{21}}{128} + \frac{5\sqrt{7+2\sqrt{21}}}{128}, \frac{21+\sqrt{21}}{128} + \frac{9\sqrt{7+2\sqrt{21}}}{128}, \frac{5\sqrt{7+2\sqrt{21}}}{128} + \frac{7+3\sqrt{21}}{128}, \frac{\sqrt{7+2\sqrt{21}}}{128} + \frac{\sqrt{21}+1}{128} \Big\}_{[-3,4]}.$$

Then by calculation we have $\mathrm{sr}(a) = 3$, $\mathrm{lpm}(a * a^\star) = 6$, and

$$\|a\|_{l_2(\mathbb{Z})} = \frac{\sqrt{1698}}{64}, \quad \mathrm{fslb}_{hp}(a) \approx 0.01424, \quad \text{and} \quad \mathrm{fslb}_{lp}(a) \approx 0.07230.$$

Applying Algorithm 3.1 with $N = 2$ to split the low-pass filter a, we obtain two auxiliary filters a^+ and a^- with $a^- = \overline{a^+}$, and

$$a^+ = \{(6.139\mathrm{E}{-}3), (2.534\mathrm{E}{-}3), (-4.206\mathrm{E}{-}2) - (6.039\mathrm{E}{-}3)\,i, (-3.166\mathrm{E}{-}2) - (2.493\mathrm{E}{-}3)\,i,$$
$$(1.292\mathrm{E}{-}1) + (4.059\mathrm{E}{-}2)\,i, (2.448\mathrm{E}{-}1) + (3.083\mathrm{E}{-}2)\,i, (1.525\mathrm{E}{-}1) - (1.218\mathrm{E}{-}1)\,i,$$
$$(2.236\mathrm{E}{-}2) - (2.368\mathrm{E}{-}1)\,i, (-1.017\mathrm{E}{-}2) - (1.661\mathrm{E}{-}1)\,i, (-2.392\mathrm{E}{-}3) - (5.277\mathrm{E}{-}2)\,i,$$
$$- (2.432\mathrm{E}{-}3)\,i, -(1.034\mathrm{E}{-}2)\,i\}_{[-3,8]}.$$

Then $\mathrm{fsp}(a^+) = \mathrm{fsp}(a^-) \approx 0.3553$, $\quad \|a^+\|_{l_2(\mathbb{Z})} = \|a^-\|_{l_2(\mathbb{Z})} \approx 0.4553$. By [21, Algorithm 4], we have a real-valued initial tight framelet filter bank $\{a; b_1, b_2\}$ with

$$b_1 = \{-6.2398\mathrm{E}{-}2, -1.0400\mathrm{E}{-}1, 4.0495\mathrm{E}{-}1, -1.1420\mathrm{E}{-}1, -1.5319\mathrm{E}{-}1, -3.9504\mathrm{E}{-}2,$$
$$3.6552\mathrm{E}{-}2, 2.6655\mathrm{E}{-}2, 5.1353\mathrm{E}{-}3\}_{[-4,4]},$$
$$b_2 = \{-2.2407\mathrm{E}{-}1, 5.1730\mathrm{E}{-}1, -2.5498\mathrm{E}{-}1, -1.0398\mathrm{E}{-}1, 2.9831\mathrm{E}{-}2, 3.0095\mathrm{E}{-}2,$$
$$5.7981\mathrm{E}{-}3\}_{[-2,4]}.$$

Applying Algorithm 4.1 with $N = 3$, we obtain high-pass filters b^+ and b^- with $b^- = \overline{b^+}$ and

$$b^+ = \{(1.167\text{E}{-}3) + (1.246\text{E}{-}3)\,i, (4.818\text{E}{-}4) + (5.144\text{E}{-}4)\,i, (-1.328\text{E}{-}2) - (1.455\text{E}{-}2)\,i,$$
$$(-8.200\text{E}{-}3) - (8.910\text{E}{-}3)\,i, (-2.118\text{E}{-}2) + (3.697\text{E}{-}2)\,i, (4.607\text{E}{-}3) + (3.039\text{E}{-}2)\,i,$$
$$(2.069\text{E}{-}1) + (5.519\text{E}{-}2)\,i, (-1.092\text{E}{-}1) - (3.182\text{E}{-}1)\,i, (-1.746\text{E}{-}1) + (2.915\text{E}{-}1)\,i,$$
$$(1.024\text{E}{-}1) - (6.285\text{E}{-}2)\,i, (1.424\text{E}{-}2) - (1.423\text{E}{-}2)\,i, (-7.223\text{E}{-}3) + (6.555\text{E}{-}3)\,i,$$
$$(3.181\text{E}{-}3) - (2.979\text{E}{-}3)\,i, (7.477\text{E}{-}4) - (7.002\text{E}{-}4)\,i\}_{[-3,8]}.$$

Then $\mathbb{CTF}_3 = \{a; b^+, b^-\}$ and $\mathbb{CTF}_4 = \{a^+, a^-; b^+, b^-\}$ are tight framelet filter banks with

$$\text{fsp}(b^+) = \text{fsp}(b^-) \approx 0.2525, \quad \text{vm}(b^+) = \text{vm}(b^-) = 3, \qquad \|b^+\|_{l_2(\mathbb{Z})} = \|b^-\|_{l_2(\mathbb{Z})} \approx 0.5410.$$

Applying Algorithm 4.2 with $N = 3$ (but $-\frac{5\pi}{12}$ in the last interval is replaced by $-\frac{\pi}{4}$ in (4.3)), we obtain filters b_1^+, b_2^+, b_1^-, and b_2^- with $b_1^- := \overline{b_1^+}$ and $b_2^- := \overline{b_2^+}$, where

$$b_1^+ = \{(1.410\text{E}{-}2) + (7.916\text{E}{-}3)\,i, (-3.633\text{E}{-}2) - (2.041\text{E}{-}2)\,i, (-2.447\text{E}{-}2) + (5.990\text{E}{-}2)\,i,$$
$$(1.102\text{E}{-}1) + (1.399\text{E}{-}2)\,i, (2.200\text{E}{-}2) - (1.600\text{E}{-}1)\,i, (-1.271\text{E}{-}1) - (1.500\text{E}{-}2)\,i,$$
$$(-3.723\text{E}{-}2) + (1.731\text{E}{-}1)\,i, (6.911\text{E}{-}2) - (1.453\text{E}{-}2)\,i, (2.012\text{E}{-}2) - (3.907\text{E}{-}2)\,i,$$
$$(2.494\text{E}{-}3) - (7.748\text{E}{-}3)\,i, (-4.307\text{E}{-}3) + (1.195\text{E}{-}3)\,i, (-4.923\text{E}{-}3) + (4.482\text{E}{-}4)\,i,$$
$$(-2.947\text{E}{-}3) + (1.260\text{E}{-}4)\,i, (-6.929\text{E}{-}4) + (2.963\text{E}{-}5)\,i\}_{[-5,8]},$$
$$b_2^+ = \{(6.146\text{E}{-}3) - (2.318\text{E}{-}2)\,i, (-1.584\text{E}{-}2) + (5.974\text{E}{-}2)\,i, (7.252\text{E}{-}2) - (7.894\text{E}{-}2)\,i,$$
$$(-2.079\text{E}{-}1) + (3.651\text{E}{-}2)\,i, (2.496\text{E}{-}1) + (1.007\text{E}{-}1)\,i, (-1.121\text{E}{-}1) - (1.787\text{E}{-}1)\,i,$$
$$(-8.903\text{E}{-}3) + (1.154\text{E}{-}1)\,i, (5.883\text{E}{-}3) - (1.417\text{E}{-}2)\,i, (2.794\text{E}{-}2) - (3.424\text{E}{-}2)\,i,$$
$$(-1.093\text{E}{-}2) + (6.816\text{E}{-}3)\,i, (-1.080\text{E}{-}2) + (1.028\text{E}{-}2)\,i, (1.011\text{E}{-}3) + (1.036\text{E}{-}3)\,i,$$
$$(2.676\text{E}{-}3) - (1.040\text{E}{-}3)\,i, (6.291\text{E}{-}4) - (2.445\text{E}{-}4)\,i\}_{[-5,8]}.$$

Then $\mathbb{CTF}_5 = \{a; b_1^+, b_2^+, b_1^-, b_2^-\}$ and $\mathbb{CTF}_6 = \{a^+, a^-; b_1^+, b_2^+, b_1^-, b_2^-\}$ are tight framelet filter banks with

$$\text{fsp}(b_1^+) = \text{fsp}(b_1^-) \approx 0.08907, \qquad \text{vm}(b_1^+) = \text{vm}(b_1^-) = 3, \qquad \|b_1^+\|_{l_2(\mathbb{Z})} = \|b_1^-\|_{l_2(\mathbb{Z})} \approx 0.3152,$$
$$\text{fsp}(b_2^+) = \text{fsp}(b_2^-) \approx 0.2371, \qquad \text{vm}(b_2^+) = \text{vm}(b_2^-) = 3, \qquad \|b_2^+\|_{l_2(\mathbb{Z})} = \|b_2^-\|_{l_2(\mathbb{Z})} \approx 0.4397.$$

See Figure 5 for the graphs of the frequency separation properties of a^+, b^+, b_1^+, and b_2^+.

Example 3. Taking $\ell = 3$, $m = 4$, and $c = 1$ in Theorem 3.3, we construct a low-pass filter a as follows:

$$a = \left\{ \frac{1+\sqrt{28}}{256} - \frac{\sqrt{8+2\sqrt{28}}}{256}, \frac{1+\sqrt{7}}{32} - \frac{3\sqrt{8+2\sqrt{28}}}{128}, \frac{7+\sqrt{28}}{64} - \frac{7\sqrt{8+2\sqrt{28}}}{128}, \frac{7-\sqrt{7}}{32} - \frac{7\sqrt{8+2\sqrt{28}}}{128}, \frac{35-5\sqrt{28}}{128}, \right.$$
$$\left. \frac{7-\sqrt{7}}{32} + \frac{7\sqrt{8+2\sqrt{28}}}{128}, \frac{7+\sqrt{28}}{64} + \frac{7\sqrt{8+2\sqrt{28}}}{128}, \frac{1+\sqrt{7}}{32} + \frac{3\sqrt{8+2\sqrt{28}}}{128}, \frac{1+\sqrt{28}}{256} + \frac{\sqrt{8+2\sqrt{28}}}{256} \right\}_{[-4,4]}.$$

Then by calculation we have $\text{sr}(a) = 4$, $\text{lpm}(a * a^\star) = 6$, and

$$\|a\|_{l_2(\mathbb{Z})} = \frac{\sqrt{25278}}{256}, \quad \text{fslb}_{hp}(a) \approx 0.004522, \quad \text{and} \quad \text{fslb}_{lp}(a) \approx 0.04163.$$

(a) $|\widehat{a}|$ and $|\widehat{a^+}|$ (b) $|\widehat{b^+}|$ (c) $|\widehat{b_1^+}|$ and $|\widehat{b_2^+}|$
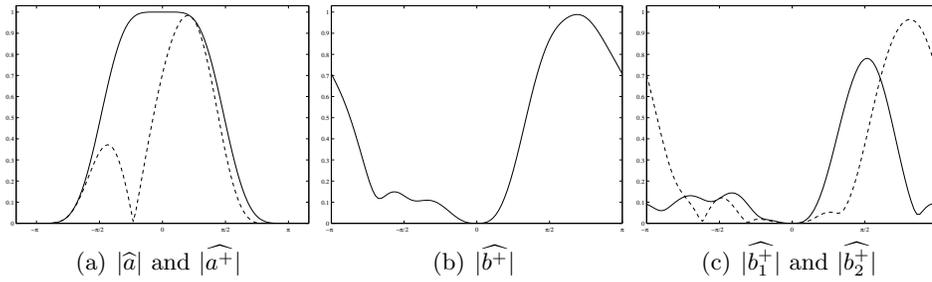
Figure 5. *The frequency separation properties of filters in Example* 2 *on the basic interval* $[-\pi, \pi]$: (a) $|\widehat{a}|$ *(solid line) and* $|\widehat{a^+}|$ *(dashed line).* (b) $|\widehat{b^+}|$. (c) $|\widehat{b_1^+}|$ *(solid line) and* $|\widehat{b_2^+}|$ *(dashed line).*

Applying Algorithm 3.1 with $N = 2$ to split the low-pass filter a, we obtain two auxiliary filters a^+ and a^- with $a^- = \overline{a^+}$, and

$$
\begin{aligned}
a^+ = \{&(3.902\mathrm{E}{-}3), (6.504\mathrm{E}{-}3), (-2.233\mathrm{E}{-}2) - (3.812\mathrm{E}{-}3)\,i, (-5.076\mathrm{E}{-}2) - (6.353\mathrm{E}{-}3)\,i, \\
&(3.532\mathrm{E}{-}2) + (2.122\mathrm{E}{-}2)\,i, (1.913\mathrm{E}{-}1) + (4.860\mathrm{E}{-}2)\,i, (2.132\mathrm{E}{-}1) - (3.118\mathrm{E}{-}2)\,i, \\
&(9.429\mathrm{E}{-}2) - (1.793\mathrm{E}{-}1)\,i, (4.639\mathrm{E}{-}3) - (2.133\mathrm{E}{-}1)\,i, (-8.165\mathrm{E}{-}3) - (1.204\mathrm{E}{-}1)\,i, \\
&(-1.573)3 - (3.704\mathrm{E}{-}2)\,i, -(8.359\mathrm{E}{-}3)\,i, -(1.610\mathrm{E}{-}3)\,i\}_{[-4,8]}.
\end{aligned}
$$

Then $\mathrm{fsp}(a^+) = \mathrm{fsp}(a^-) \approx 0.3321$ and $\|a^+\|_{l_2(\mathbb{Z})} = \|a^-\|_{l_2(\mathbb{Z})} \approx 0.4392$. By [21, Algorithm 4], we have a real-valued initial tight framelet filter bank $\{a; b_1, b_2\}$ with

$$
\begin{aligned}
b_1 = \{&(-2.2407\mathrm{E}{-}1), (5.1730\mathrm{E}{-}1), (-2.5498\mathrm{E}{-}1), (-1.0398\mathrm{E}{-}1), (2.9831\mathrm{E}{-}2), (3.0095\mathrm{E}{-}2), \\
&(5.7981\mathrm{E}{-}3)\}_{[-2,4]}, \\
b_2 = \{&(-6.2398\mathrm{E}{-}2), (-1.0400\mathrm{E}{-}1), (4.0495\mathrm{E}{-}1), (-1.1420\mathrm{E}{-}1), (-1.5319\mathrm{E}{-}1), \\
&(-3.9504\mathrm{E}{-}2), (3.6552\mathrm{E}{-}2), (2.6655\mathrm{E}{-}2), (5.1353\mathrm{E}{-}3)\}_{[-4,4]}.
\end{aligned}
$$

Applying Algorithm 4.1 with $N = 3$, we obtain high-pass filters b^+ and b^- with $b^- = \overline{b^+}$ and

$$
\begin{aligned}
b^+ = \{&(-1.878\mathrm{E}{-}2) - (2.707\mathrm{E}{-}2)\,i, (4.053\mathrm{E}{-}3) + (5.841\mathrm{E}{-}3)\,i, (4.060\mathrm{E}{-}2) - (7.186\mathrm{E}{-}2)\,i, \\
&(1.588\mathrm{E}{-}1) + (2.570\mathrm{E}{-}1)\,i, (-3.738\mathrm{E}{-}1) - (6.193\mathrm{E}{-}2)\,i, (1.643\mathrm{E}{-}1) - (1.824\mathrm{E}{-}1)\,i, \\
&(2.408\mathrm{E}{-}2) + (4.820\mathrm{E}{-}2)\,i, (1.778\mathrm{E}{-}2) + (2.721\mathrm{E}{-}2)\,i, (-4.391\mathrm{E}{-}3) + (2.222\mathrm{E}{-}3)\,i, \\
&(-6.987\mathrm{E}{-}3) - (2.480\mathrm{E}{-}4)\,i, (-3.872\mathrm{E}{-}3) + (1.705\mathrm{E}{-}3)\,i, (-1.525\mathrm{E}{-}3) + (1.058\mathrm{E}{-}3)\,i, \\
&(-2.938\mathrm{E}{-}4) + (2.038\mathrm{E}{-}4)\,i\}_{[-6,6]}.
\end{aligned}
$$

Then $\mathbb{CTF}_3 = \{a; b^+, b^-\}$ and $\mathbb{CTF}_4 = \{a^+, a^-; b^+, b^-\}$ are tight framelet filter banks with

$$
\mathrm{fsp}(b^+) = \mathrm{fsp}(b^-) \approx 0.1715, \quad \mathrm{vm}(b^+) = \mathrm{vm}(b^-) = 3, \quad \|b^+\|_{l_2(\mathbb{Z})} = \|b^-\|_{l_2(\mathbb{Z})} \approx 0.5542.
$$

Applying Algorithm 4.2 with $N = 4$, we obtain finitely supported filters b_1^+, b_2^+, b_1^-, and b_2^-

(a) $|\hat{a}|$ and $|\widehat{a^+}|$ (b) $|\widehat{b^+}|$ (c) $|\widehat{b_1^+}|$ and $|\widehat{b_2^+}|$
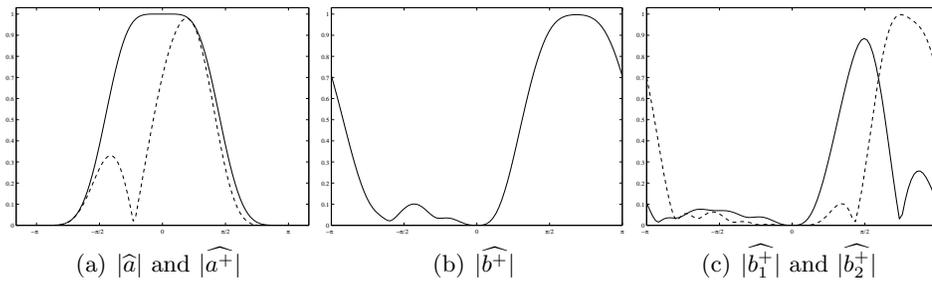
Figure 6. *The frequency separation properties of filters in Example 3 on the basic interval $[-\pi, \pi]$: (a) $|\hat{a}|$ (solid line) and $|\widehat{a^+}|$ (dashed line). (b) $|\widehat{b^+}|$. (c) $|\widehat{b_1^+}|$ (solid line) and $|\widehat{b_2^+}|$ (dashed line).*

with $b_1^- := \overline{b_1^+}$ and $b_2^- := \overline{b_2^+}$, where

$$
\begin{aligned}
b_1^+ = \{&(-1.745\mathrm{E}{-}2) + (9.693\mathrm{E}{-}3)\,i, (6.491\mathrm{E}{-}2) + (5.688\mathrm{E}{-}2)\,i, (3.833\mathrm{E}{-}2) - (1.242\mathrm{E}{-}1)\,i,\\
&(-1.287\mathrm{E}{-}1) - (6.067\mathrm{E}{-}2)\,i, (-7.018\mathrm{E}{-}2) + (1.205\mathrm{E}{-}1)\,i, (6.844\mathrm{E}{-}2) + (1.123\mathrm{E}{-}1)\,i,\\
&(1.050\mathrm{E}{-}1) - (8.187\mathrm{E}{-}2)\,i, (-5.598\mathrm{E}{-}2) - (7.211\mathrm{E}{-}2)\,i, (-5.993\mathrm{E}{-}3) + (3.987\mathrm{E}{-}2)\,i,\\
&(1.544\mathrm{E}{-}2) - (7.127\mathrm{E}{-}3)\,i, (-6.767\mathrm{E}{-}3) + (3.341\mathrm{E}{-}3)\,i, (-5.880\mathrm{E}{-}3) + (2.845\mathrm{E}{-}3)\,i,\\
&(-1.133\mathrm{E}{-}3) + (5.481\mathrm{E}{-}4)\,i, \}_{[-4,8]},\\
b_2^+ = \{&(-3.576\mathrm{E}{-}2) - (6.860\mathrm{E}{-}3)\,i, (9.263\mathrm{E}{-}2) + (7.157\mathrm{E}{-}2)\,i, (-4.133\mathrm{E}{-}2) - (1.877\mathrm{E}{-}1)\,i,\\
&(-1.050\mathrm{E}{-}1) + (2.156\mathrm{E}{-}1)\,i, (1.890\mathrm{E}{-}1) - (1.173\mathrm{E}{-}1)\,i, (-1.623\mathrm{E}{-}1) - (8.414\mathrm{E}{-}3)\,i,\\
&(6.404\mathrm{E}{-}2) + (6.341\mathrm{E}{-}2)\,i, (8.514\mathrm{E}{-}3) - (7.802\mathrm{E}{-}3)\,i, (7.322\mathrm{E}{-}3) - (4.871\mathrm{E}{-}2)\,i,\\
&(-2.410\mathrm{E}{-}2) + (2.722\mathrm{E}{-}2)\,i, (2.080\mathrm{E}{-}3) + (1.630\mathrm{E}{-}3)\,i, (4.058\mathrm{E}{-}3) - (2.181\mathrm{E}{-}3)\,i,\\
&(7.818\mathrm{E}{-}4) - (4.203\mathrm{E}{-}4)\,i\}_{[-4,8]}.
\end{aligned}
$$

Then $\mathbb{CTF}_5 = \{a; b_1^+, b_2^+, b_1^-, b_2^-\}$ and $\mathbb{CTF}_6 = \{a^+, a^-; b_1^+, b_2^+, b_1^-, b_2^-\}$ are tight framelet filter banks with

$$
\begin{aligned}
\mathrm{fsp}(b_1^+) = \mathrm{fsp}(b_1^-) \approx 0.0233, \quad & \mathrm{vm}(b_1^+) = \mathrm{vm}(b_1^-) = 3, \quad & \|b_1^+\|_{l_2(\mathbb{Z})} = \|b_1^-\|_{l_2(\mathbb{Z})} \approx 0.3313,\\
\mathrm{fsp}(b_2^+) = \mathrm{fsp}(b_2^-) \approx 0.1584, \quad & \mathrm{vm}(b_2^+) = \mathrm{vm}(b_2^-) = 3, \quad & \|b_2^+\|_{l_2(\mathbb{Z})} = \|b_2^-\|_{l_2(\mathbb{Z})} \approx 0.4442.
\end{aligned}
$$

See Figure 6 for the graphs of the frequency separation properties of a^+, b^+, b_1^+, and b_2^+.

5. Numerical experiments on image denoising and inpainting. In this section, we test the performance of our directional compactly supported TP^c-$\mathbb{CTF}_n$ constructed in section 4 for the image denoising and inpainting problems. We deal with the model problems with only standard Gaussian noise. We compare their performance with their band-limited counterparts as well as several other transform-based methods such as curvelets and shearlets. See [7, 10, 11, 16, 18, 19, 21, 36] on tight wavelet frames and see [3, 12, 13, 14, 29, 31, 34, 35, 41] for curvelets and shearlets as well as their applications. See [24, 25, 26, 39] for detailed comparison results on the performance of directional band-limited TP^b-$\mathbb{CTF}_n$ with several other transform-based methods.

(a) Barbara   (b) Flintstones   (c) Fingerprint   (d) Boat   (e) Pentagon

(f) Text 1   (g) Text 2   (h) 50% Random   (i) 80% Random
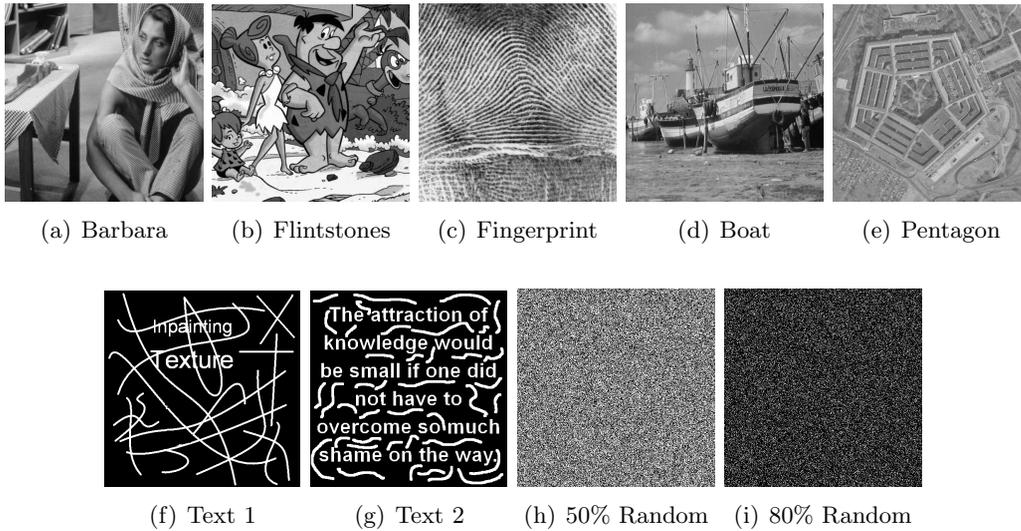
Figure 7. (a)–(e) *are the five* 512×512 *gray-scale testing images: Barbara, Flintstones, Fingerprint, Boat, and Pentagon.* (f)–(i) *are the four* 512×512 *inpainting masks: Text* 1*, Text* 2*, 50% Random Pixel Lost, and 80% Random Pixel Lost.*

The directional compactly supported $\text{TP}^c\text{-}\mathbb{C}\text{TF}_4$ and $\text{TP}^c\text{-}\mathbb{C}\text{TF}_6$ which will be used in this section for comparison are from Examples 1–3. The testing images *Barbara*, *Flintstones* (cartoon image), *Fingerprint*, *Boat*, and *Pentagon* (cartoonlike image) are given in Figure 7, and all of them are 512×512 gray-scale images. The masks (*Text* 1, *Text* 2, 50% *Random Pixel Lost*, and 80% *Random Pixel Lost*) for the inpainting problem are also given in Figure 7. As usual, we use PSNR to measure the quality of image restoration, which is defined to be $\text{PSNR}(I, \mathring{I}) = 10 \log_{10} \frac{255^2}{\text{MSE}(I - \mathring{I})}$, where I is the original/true image, $\mathring{I}$ is a denoised/reconstructed image, and $\text{MSE}(\cdot)$ is the mean squared error.

The implementation of directional compactly supported $\text{TP}^c\text{-}\mathbb{C}\text{TF}_n$ with $n = 3, 4, 5, 6$ in this paper and the numerical experiments in this section have been made available as a MATLAB package `cptTPCTF` that can be found in: http://staffweb1.cityu.edu.hk/xzhuang7.

5.1. Image denoising. In all denoising experiments with DT-$\mathbb{C}$WT, $\text{TP}^c\text{-}\mathbb{C}\text{TF}_n$, and $\text{TP}^b\text{-}\mathbb{C}\text{TF}_n$, bivariate shrinkage in [38] with window size 7×7 is applied to the framelet coefficients. The level of decomposition is set to be $J = 5$ for all the directional tensor product complex tight framelets, while the level of decomposition is set to be $J = 6$ for the DT-$\mathbb{C}$WT in [28, 37]. We use mirror symmetry extension for all the test images to handle the boundary effect.

We compare the performance of image denoising in three groups according to different number of directions in the system. The first group (Group I) with 4 directions employs directional band-limited $\text{TP}^b\text{-}\mathbb{C}\text{TF}_3$ in [24, 25] and directional compactly supported $\text{TP}^c\text{-}\mathbb{C}\text{TF}_3$ constructed in Example 1 (same as Example 3 in [23]). The second group (Group II) with 6 directions employs directional band-limited $\text{TP}^b\text{-}\mathbb{C}\text{TF}_4$ in [24, 25], directional compactly supported $\text{TP}^c\text{-}\mathbb{C}\text{TF}_4$ constructed in Example 3, and DT-$\mathbb{C}$WT in [28, 37]. The third group

(Group III) with more directions employs directional band-limited TP^b-$\mathbb{CTF}_6$ in [24, 25], directional compactly supported TP^c-$\mathbb{CTF}_6$ constructed in Examples 2 and 3, and two other nontensor product based approaches including curvelets in [3] and shearlets in [34, 35]. We download both software for curvelets and compactly supported shearlets packages from the corresponding authors' homepages and run denoising code for test images. We choose the frequency wrapping package from CurveLab (v2.1.3) at http://www.curvelet.org for curvelet comparison, and the DNST (4 scales, redundancy 49) in ShearLab3D (v1.01) [30] at http://www.shearlab.org for shearlet comparison. We remark that other related packages exists, such as the local shearlet toolbox [13], ShearLab based on pseudopolar coordinates [12, 31], fast finite shearlet transform [27], steerable pyramids [40], and ridgelets[4].

See Table 2 for image denoising comparison for independent identically distributed (i.i.d.) white Gaussian noise with standard deviation $\sigma = 5, 10, 25, 40, 50, 80, 100, 120, 150, 180, 200$. As usual, the standard deviation for Gaussian noise is assumed to be known in advance. Moreover, a reference column using BM3D [8] is included. Note that BM3D is a patch-based method and uses more sophisticated techniques [32].

Table 2 indicates that image denoising results by directional compactly supported tensor product complex tight framelets are comparable to those by directional band-limited tensor product complex tight framelets for both TP^b-$\mathbb{CTF}_4$ and TP^b-$\mathbb{CTF}_6$. In particular, the performance of directional compactly supported TP^c-$\mathbb{CTF}_4$ is comparable to DT-$\mathbb{CWT}$ and hence the directional compactly supported TP^c-$\mathbb{CTF}_4$ constructed in this paper offers an alternative to the popular DT-$\mathbb{CWT}$ in [37]. The performance of BM3D is superior when the noise level is low while it does not perform well when the noise level is high.

5.2. Image inpainting. Directional band-limited TP^b-$\mathbb{CTF}_6$ has been applied to image inpainting in [39] with impressive performance compared with many other image inpainting algorithms. Here we simply apply the same inpainting algorithm in [39] while replacing the directional band-limited TP^b-$\mathbb{CTF}_6$ transform with directional compactly supported TP^c-$\mathbb{CTF}_6$ constructed in section 4. Similarly to most other transform-based image inpainting algorithms, the algorithm in [39] applies iterative thresholding with decreasing threshold values. See [39] for the detail of this image inpainting algorithm. We only report in Table 3 the performance for image inpainting using directional compactly supported TP^c-$\mathbb{CTF}_6$ in Example 3 and directional band-limited TP^b-$\mathbb{CTF}_6$ in [39]. For comparisons among TP^b-$\mathbb{CTF}_6$ and other transform-based algorithms (e.g., DCT-Haar [33]), we refer to the detailed experimental reports in [25, 39].

The algorithm developed in [39] not only has impressive performance in image inpainting without noise but also works well and stably for image inpainting with additive white Gaussian noise. Similarly to the image denoising problem, we assume that the noise standard deviation σ is known in advance for image inpainting with noise. Table 3 demonstrates that the performance of compactly supported TP^c-$\mathbb{CTF}_6$ is comparable to that of band-limited TP^b-$\mathbb{CTF}_6$ in the image inpainting problem.

In conclusion, the proposed directional compactly supported TP^c-$\mathbb{CTF}_n$ are comparable to their band-limited counterparts, leading to efficient computational algorithms and good space/frequency localization property. The directional compactly supported TP^c-$\mathbb{CTF}_4$ with 6 directions in two dimensions offers an alternative to the popular DT-$\mathbb{CWT}$, and the directional

Table 2

Image denoising comparison results in terms of PSNR. σ in Column #0 is the standard deviation of the i.i.d. Gaussian noise. We put results of BM3D in Column #1 as a reference column. Column #2 uses the directional compactly supported TP^c-$\mathbb{C}\mathrm{TF}_3$. Column #3 uses the directional band-limited TP^b-$\mathbb{C}\mathrm{TF}_3$ constructed in Example 1. Column #4 uses the directional compactly supported TP^c-$\mathbb{C}\mathrm{TF}_4$ constructed in Example 3. Column #5 uses the directional band-limited TP^b-$\mathbb{C}\mathrm{TF}_4$. Column #6 uses the DT-$\mathbb{C}$WT in [37]. Columns #7 and #8 use the directional compactly supported TP^c-$\mathbb{C}\mathrm{TF}_6$ constructed in Examples 2 and 3. Column #9 uses the directional band-limited TP^b-$\mathbb{C}\mathrm{TF}_6$. Column #10 uses the curvelet (the warping package), and Column#11 uses shearlets (DNST).

0	1	2	3	4	5	6	7	8	9	10	11
		Group I		Group II			Group III				
σ	BM3D [8]	TP^c-$\mathbb{C}\mathrm{TF}_3$ Ex. 1	TP^b-$\mathbb{C}\mathrm{TF}_3$ [24, 25]	TP^c-$\mathbb{C}\mathrm{TF}_4$ Ex. 3	TP^b-$\mathbb{C}\mathrm{TF}_4$ [24, 25]	DT-$\mathbb{C}$WT [37]	TP^c-$\mathbb{C}\mathrm{TF}_6$ Ex. 2	TP^c-$\mathbb{C}\mathrm{TF}_6$ Ex. 3	TP^b-$\mathbb{C}\mathrm{TF}_6$ [24, 25]	CurveLab [3]	DNST [35]
512×512 Flintstones											
5	36.17	35.47	35.40	35.50	35.48	35.58	35.52	35.61	35.61	32.15	34.50
10	32.45	31.10	30.97	31.20	31.17	31.29	31.38	31.43	31.46	28.84	31.19
25	28.63	26.49	26.44	26.73	26.75	26.76	26.96	27.04	27.16	25.16	27.29
40	26.11	24.26	24.29	24.51	24.55	24.55	24.66	24.76	24.95	23.07	25.12
50	25.11	23.19	23.26	23.43	23.49	23.48	23.53	23.62	23.85	22.04	24.02
80	22.56	20.91	21.07	21.14	21.24	21.22	21.12	21.20	21.46	19.86	21.61
100	21.32	19.84	20.04	20.06	20.18	20.13	20.01	20.09	20.34	18.86	20.44
120	20.29	18.97	19.22	19.20	19.33	19.27	19.14	19.21	19.44	18.11	19.49
150	18.48	17.97	18.22	18.19	18.32	18.26	18.13	18.19	18.39	17.27	18.33
180	17.37	17.21	17.44	17.42	17.53	17.48	17.37	17.42	17.57	16.44	17.43
200	16.90	16.81	17.02	17.00	17.10	17.05	16.95	16.99	17.13	16.08	16.91
512×512 Barbara											
5	38.31	37.02	37.16	37.23	37.42	37.37	37.53	37.72	37.84	33.81	37.17
10	34.98	32.98	33.19	33.36	33.65	33.54	33.80	34.04	34.18	29.17	33.62
25	30.72	27.84	28.04	28.41	28.77	28.74	28.98	29.25	29.35	24.84	28.93
40	27.99	25.33	25.53	25.94	26.29	26.34	26.49	26.75	26.86	23.86	26.48
50	27.23	24.29	24.48	24.89	25.21	25.25	25.37	25.61	25.71	23.41	25.31
80	24.79	22.67	22.82	23.03	23.21	23.20	23.26	23.44	23.53	22.29	22.96
100	23.62	22.11	22.25	22.34	22.45	22.39	22.44	22.56	22.64	21.61	22.06
120	22.66	21.68	21.82	21.86	21.91	21.80	21.87	21.94	22.00	21.07	21.35
150	20.71	21.15	21.30	21.29	21.30	21.15	21.22	21.27	21.31	20.44	20.47
180	19.32	20.69	20.84	20.82	20.79	20.63	20.70	20.73	20.75	19.79	19.69
200	18.69	20.42	20.57	20.53	20.50	20.31	20.40	20.41	20.42	19.45	19.21
512×512 Boat											
5	37.28	36.52	36.45	36.56	36.53	36.78	36.82	36.86	36.92	33.57	36.04
10	33.92	33.03	32.97	33.13	33.10	33.22	33.30	33.35	33.41	30.59	33.15
25	29.91	28.94	28.98	29.09	29.06	29.02	29.08	29.12	29.26	27.51	29.23
40	27.74	26.87	26.98	27.03	27.03	26.97	26.99	27.02	27.19	25.91	27.20
50	26.78	25.95	26.07	26.11	26.12	26.06	26.05	26.08	26.25	25.16	26.23
80	24.86	24.15	24.29	24.33	24.33	24.26	24.26	24.28	24.41	23.51	24.17
100	23.97	23.36	23.50	23.55	23.53	23.45	23.46	23.48	23.58	22.88	23.17
120	23.25	22.76	22.88	22.93	22.90	22.80	22.83	22.85	22.91	22.07	22.33
150	21.64	22.05	22.17	22.21	22.16	22.02	22.09	22.10	22.12	21.41	21.26
180	20.19	21.51	21.62	21.64	21.56	21.39	21.49	21.50	21.48	20.69	20.34
200	19.52	21.20	21.31	21.32	21.21	21.03	21.15	21.15	21.12	20.31	19.79
512×512 Fingerprint											
5	36.51	35.51	35.29	35.56	35.56	35.93	36.19	36.26	36.27	33.36	35.28
10	32.46	31.18	30.97	31.40	31.42	31.88	32.21	32.23	32.10	30.62	31.76
25	27.70	26.69	26.56	27.01	27.00	27.34	27.35	27.34	26.98	26.07	27.10
40	25.30	24.63	24.75	24.96	24.93	25.00	25.07	25.07	24.68	23.97	24.82
50	24.53	23.57	23.84	23.95	23.95	23.96	24.04	24.05	23.67	23.00	23.78
80	22.56	21.27	21.73	21.79	21.92	21.91	21.93	21.99	21.66	21.23	21.63
100	21.61	20.21	20.69	20.77	21.01	21.01	20.96	21.03	20.75	20.48	20.56
120	20.77	19.39	19.87	19.98	20.30	20.29	20.17	20.26	20.01	19.73	19.66
150	18.34	18.43	18.92	19.04	19.47	19.40	19.23	19.35	19.10	18.81	18.54
180	17.24	17.70	18.22	18.31	18.80	18.67	18.48	18.62	18.37	18.11	17.63
200	16.83	17.31	17.85	17.90	18.41	18.24	18.06	18.22	17.96	17.67	17.12
512×512 Pentagon											
5	35.63	35.20	35.14	35.22	35.21	35.22	35.23	35.24	35.24	31.64	33.68
10	31.36	30.70	30.63	30.77	30.72	30.85	30.78	30.79	30.82	27.90	29.78
25	26.81	26.08	26.15	26.24	26.25	26.44	26.26	26.32	26.43	25.01	26.18
40	25.12	24.43	24.53	24.59	24.66	24.76	24.63	24.69	24.79	24.07	24.79
50	24.40	23.84	23.95	24.00	24.07	24.13	24.03	24.08	24.17	23.56	24.17
80	23.15	22.78	22.88	22.93	23.02	23.00	22.96	22.99	23.03	22.56	22.84
100	22.57	22.29	22.40	22.46	22.53	22.49	22.46	22.47	22.51	22.01	22.15
120	22.10	21.90	22.00	22.06	22.13	22.06	22.05	22.05	22.07	21.59	21.55
150	21.01	21.43	21.53	21.57	21.61	21.51	21.52	21.51	21.53	21.06	20.75
180	20.02	21.04	21.15	21.16	21.17	21.04	21.08	21.07	21.07	20.64	20.01
200	19.49	20.81	20.92	20.93	20.91	20.75	20.83	20.81	20.79	20.39	19.54

Table 3

Performance in terms of PSNR values for image inpainting with Gaussian noise at standard deviation level $\sigma = 0$ (no noise), $10, 20, 30, 40, 50$. All the results are obtained from the same inpainting algorithm in [39], where columns of $\mathrm{TP}^b\text{-}\mathbb{CTF}_6$ apply band-limited $\mathrm{TP}^b\text{-}\mathbb{CTF}_6$ in [39] while columns of $\mathrm{TP}^c\text{-}\mathbb{CTF}_6$ apply $\mathrm{TP}^c\text{-}\mathbb{CTF}_6$ constructed in Example 3.

	Text 1		Text 2		50% random lost		80% random lost	
σ	$\mathrm{TP}^c\text{-}\mathbb{CTF}_6$ Ex. 3	$\mathrm{TP}^b\text{-}\mathbb{CTF}_6$ [39]	$\mathrm{TP}^c\text{-}\mathbb{CTF}_6$ Ex. 3	$\mathrm{TP}^b\text{-}\mathbb{CTF}_6$ [39]	$\mathrm{TP}^c\text{-}\mathbb{CTF}_6$ Ex. 3	$\mathrm{TP}^b\text{-}\mathbb{CTF}_6$ [39]	$\mathrm{TP}^c\text{-}\mathbb{CTF}_6$ Ex. 3	$\mathrm{TP}^b\text{-}\mathbb{CTF}_6$ [39]
	512×512 Barbara							
0	35.22	36.59	31.97	32.68	34.90	35.73	27.12	28.16
10	31.37	31.81	29.56	29.85	30.81	31.11	25.95	26.70
20	28.76	28.99	27.55	27.71	27.68	28.00	24.17	24.70
30	27.00	27.18	26.08	26.24	25.63	25.95	22.92	23.34
40	25.73	25.88	24.99	25.14	24.27	24.56	22.21	22.45
50	24.77	24.91	24.16	24.30	23.36	23.60	21.73	21.90
	512×512 Flintstones							
0	29.22	29.59	24.96	25.35	30.52	30.64	24.15	24.40
10	27.14	27.42	24.07	24.40	27.99	28.05	23.32	23.49
20	25.40	25.64	22.99	23.26	25.72	25.89	21.93	22.16
30	24.12	24.35	22.08	22.34	24.01	24.27	20.70	20.99
40	23.08	23.31	21.29	21.55	22.65	22.99	19.69	20.01
50	22.20	22.45	20.61	20.87	21.53	21.92	18.90	19.20
	512×512 Fingerprint							
0	31.88	31.35	28.15	27.78	34.14	34.12	26.93	26.00
10	28.82	28.46	26.60	26.24	29.25	28.88	25.22	24.12
20	26.53	26.20	25.06	24.72	26.27	25.76	23.33	22.49
30	25.03	24.70	23.93	23.59	24.53	24.07	22.05	21.51
40	23.95	23.61	23.05	22.72	23.32	22.91	21.05	20.68
50	23.10	22.76	22.32	22.00	22.38	22.01	20.23	19.96
	512×512 Boat							
0	34.68	34.96	30.56	30.80	34.15	34.42	28.42	28.58
10	30.89	31.04	28.65	28.80	30.51	30.65	26.99	27.08
20	28.69	28.84	27.17	27.32	28.00	28.20	25.39	25.56
30	27.24	27.41	26.09	26.24	26.41	26.66	24.21	24.46
40	26.20	26.38	25.27	25.43	25.33	25.56	23.42	23.60
50	25.41	25.57	24.61	24.80	24.51	24.75	22.80	22.96
	512×512 Pentagon							
0	32.65	32.81	29.93	30.08	28.69	28.69	25.12	25.10
10	28.71	28.81	27.53	27.62	26.88	26.91	24.39	24.41
20	26.26	26.37	25.63	25.74	25.21	25.35	23.67	23.85
30	24.97	25.09	24.53	24.67	24.21	24.34	23.06	23.20
40	24.20	24.31	23.84	23.96	23.57	23.70	22.53	22.65
50	23.67	23.77	23.36	23.46	23.09	23.21	22.07	22.21

compactly supported $\mathrm{TP}^c\text{-}\mathbb{CTF}_6$ often outperforms several other transform-based methods in image denoising and inpainting.

6. Conclusions and further remarks. In this paper, for a given eligible low-pass filter, we provide general algorithms for the construction of directional compactly supported tensor product complex tight framelets $\mathrm{TP}^c\text{-}\mathbb{CTF}_n$ with $n = 3, 4, 5, 6$. We employ our proposed algorithms to find several concrete examples of directional compactly supported $\mathrm{TP}^c\text{-}\mathbb{CTF}_n$ with $n = 3, 4, 5, 6$ such that they have good performance in image denoising and inpainting.

Despite the fact that we are applying optimization techniques in our algorithms for constructing $\mathrm{TP}^c\text{-}\mathbb{CTF}_n$ with $n = 3, 4, 5, 6$, we do not claim in this paper that we are able to find the "optimal" directional compactly supported $\mathrm{TP}^c\text{-}\mathbb{CTF}_n$ with the "best" possible performance for image processing. Instead, we are trying to find reasonably good examples of directional compactly supported $\mathrm{TP}^c\text{-}\mathbb{CTF}_n$ with $n = 3, 4, 5, 6$ such that they perform comparably to their band-limited counterparts in [24, 25, 39]. Tables 2 and 3 confirm the effectiveness of our approach in this paper. Moreover, to compare the bandlimited $\mathrm{TP}^b\text{-}\mathbb{CTF}_6$ in [24, 25, 39] and the compactly supported $\mathrm{TP}^c\text{-}\mathbb{CTF}_6$ in Example 3, Figure 8 shows a similar pattern of the frequency responses between these two complex tight framelets, which more or less explains the comparable performance of these two types of complex tight framelets. Table 4 further
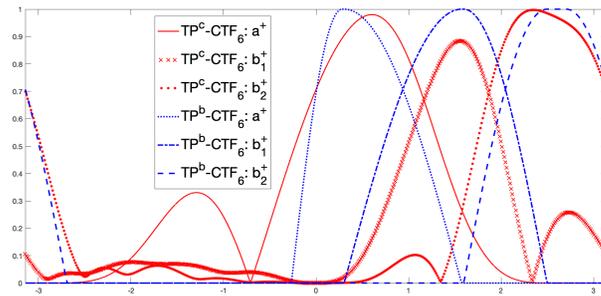
Figure 8. *Frequency responses of the filters a^+, b_1^+, b_2^+ in the compactly supported $\mathbb{C}TF_6$ of Example 3 (red) and their corresponding filters in the band-limited $\mathbb{C}TF_6$ of [24, 25] (blue).*

Table 4
Comparison of compactly supported $\mathbb{C}TF_6 = \{a^+, a^-; b_1^+, b_1^-, b_2^+, b_2^-\}$ in Example 3 and band-limited $\mathbb{C}TF_6$ in [24, 25]. The quantities $\mathrm{E}(u), \mathrm{Var}(u), \mathrm{fsp}(u), \|u\|_{l_2(\mathbb{Z})}$ are the expectation, the variance, the frequency separation quantity, and the l_2-norm of a filter u, respectively.

u	$\mathrm{E}(u)$	$\mathrm{Var}(u)$	$\mathrm{fsp}(u)$	$\|u\|_{l_2(\mathbb{Z})}$	$\mathrm{E}(u)$	$\mathrm{Var}(u)$	$\mathrm{fsp}(u)$	$\|u\|_{l_2(\mathbb{Z})}$
	\multicolumn{4}{c}{$\mathrm{TP}^c\text{-}\mathbb{C}TF_6$ in Example 3}	\multicolumn{4}{c}{$\mathrm{TP}^b\text{-}\mathbb{C}TF_6$ in [24, 25]}			
a^+	2.6692	1.9223	0.3321	0.4392	0	3.4741	0.1069	0.3847
b_1^+	0.0764	3.2903	0.0233	0.3313	0	2.1231	0	0.4195
b_2^+	−0.599	2.0891	0.1584	0.4442	0	2.4819	0.1476	0.4195

compares several quantities of these two complex tight framelets. In terms of expectation, the low-pass filter in $\mathrm{TP}^b\text{-}\mathbb{C}TF_6$ has zero mean while the low-pass filter in $\mathrm{TP}^c\text{-}\mathbb{C}TF_6$ doesn't. Though band-limited $\mathrm{TP}^b\text{-}\mathbb{C}TF_n$ have infinite vanishing moments, they have infinite support, which could lead to high variance of their filters. Table 4 shows that filters in $\mathrm{TP}^c\text{-}\mathbb{C}TF_6$ have smaller variances in general compared to those in $\mathrm{TP}^b\text{-}\mathbb{C}TF_6$. For the frequency separation property, being band-limited, $\mathrm{TP}^b\text{-}\mathbb{C}TF_6$ has better frequency separation between low pass and high pass filters and, as expected, band-limited $\mathrm{TP}^b\text{-}\mathbb{C}TF_6$ has better frequency separation quantities than compactly supported $\mathrm{TP}^c\text{-}\mathbb{C}TF_6$. Using further refinement of these quantities and advanced optimization techniques could lead to further improved compactly supported $\mathrm{TP}^c\text{-}\mathbb{C}TF_n$.

In comparison with band-limited $\mathrm{TP}^b\text{-}\mathbb{C}TF_n$ in [24, 25, 39], our constructed spatially compactly supported $\mathrm{TP}^c\text{-}\mathbb{C}TF_n$ lead to more computationally efficient algorithms for their applications in multidimensional problems. In view of their tensor product nature, our compactly supported $\mathbb{C}TF_n$ could be easily applied to higher-dimensional problems such as video processing, seismic data processing, etc., through a simple tensor product process. One can also build $\mathbb{C}TF_n$ with $n \geqslant 6$ following an approach similar to Algorithm 4.2. However, the performance improvement could be limited.

Mirror symmetry extension of an image is often adopted for transform-based methods to handle the boundary effect. Consequently, the boundary wavelets or framelets can have no more than one vanishing moment and hence lose effectiveness and sparsity near the boundaries of an image. To remedy this shortcoming of boundary effect suffered by most transform-based methods for image processing, our constructed one-dimensional compactly supported $\mathbb{C}TF_n$ are particularly appealing to be adapted to the interval $[0, 1]$ with high vanishing moments.

Then simply employing the tensor product, we can obtain directional tensor product complex tight framelets in $[0,1]^d$ with boundary framelets having high vanishing moments, which are much desired to reduce/eliminate the boundary effects for improving performance in image processing. Due to the complexity of adapting tight framelets to bounded intervals, we shall address such an issue elsewhere.

7. Proofs of theorems in section 3. This section provides detailed proofs for theorems (Theorems 3.1, 3.2, and 3.3) in section 3.

Proof of Theorem 3.1. Since $\widehat{a}$ is 2π-periodic, it is trivial to observe that the conditions in (3.1) are equivalent to

$$(7.1) \qquad |\widehat{a^+}(\xi)|^2 + |\widehat{a^-}(\xi)|^2 = |\widehat{a}(\xi)|^2,$$

$$(7.2) \qquad |\widehat{a^+}(\xi+\pi)|^2 + |\widehat{a^-}(\xi+\pi)|^2 = |\widehat{a}(\xi+\pi)|^2,$$

$$(7.3) \qquad \widehat{a^+}(\xi)\overline{\widehat{a^+}(\xi+\pi)} + \widehat{a^-}(\xi)\overline{\widehat{a^-}(\xi+\pi)} = \widehat{a}(\xi)\overline{\widehat{a}(\xi+\pi)}$$

for almost every $\xi \in [0,\pi]$. In the rest of this proof, we assume $\xi \in [0,\pi]$. Then (7.1) and (7.2) imply

$$|\widehat{a^+}(\xi)|^2 = |\widehat{a}(\xi)|^2 - |\widehat{a^-}(\xi)|^2, \qquad |\widehat{a^-}(\xi+\pi)|^2 = |\widehat{a}(\xi+\pi)|^2 - |\widehat{a^+}(\xi+\pi)|^2.$$

Thus, by (7.3) and the above identities, applying the Cauchy–Schwarz inequality, for $\xi \in [0,\pi]$, we have

$$
\begin{aligned}
|\widehat{a}(\xi)\widehat{a}(\xi+\pi)|^2 &= \left| \overline{\widehat{a^+}(\xi+\pi)}\widehat{a^+}(\xi) + \widehat{a^-}(\xi)\overline{\widehat{a^-}(\xi+\pi)} \right|^2 \\
&\leqslant \left(|\widehat{a^+}(\xi+\pi)|^2 + |\widehat{a^-}(\xi)|^2 \right) \left(|\widehat{a^+}(\xi)|^2 + |\widehat{a^-}(\xi+\pi)|^2 \right) \\
&= \left(|\widehat{a^+}(\xi+\pi)|^2 + |\widehat{a^-}(\xi)|^2 \right) \left(|\widehat{a}(\xi)|^2 - |\widehat{a^-}(\xi)|^2 + |\widehat{a}(\xi+\pi)|^2 - |\widehat{a^+}(\xi+\pi)|^2 \right).
\end{aligned}
$$

Let $F(\xi) := |\widehat{a^+}(\xi+\pi)|^2 + |\widehat{a^-}(\xi)|^2$. Then the above inequality can be rewritten as

$$|\widehat{a}(\xi)\widehat{a}(\xi+\pi)|^2 \leqslant F(\xi)\left(|\widehat{a}(\xi)|^2 + |\widehat{a}(\xi+\pi)|^2 - F(\xi) \right).$$

Solving the above inequality for $F(\xi)$ and noting $F(\xi) \geqslant 0$, we conclude that

$$
\begin{aligned}
F(\xi) &\geqslant \frac{|\widehat{a}(\xi)|^2 + |\widehat{a}(\xi+\pi)|^2 - \sqrt{(|\widehat{a}(\xi)|^2 + |\widehat{a}(\xi+\pi)|^2)^2 - 4|\widehat{a}(\xi)\widehat{a}(\xi+\pi)|^2}}{2} \\
&= \frac{|\widehat{a}(\xi)|^2 + |\widehat{a}(\xi+\pi)|^2 - \left| |\widehat{a}(\xi)|^2 - |\widehat{a}(\xi+\pi)|^2 \right|}{2} \\
&= \min(|\widehat{a}(\xi)|^2, |\widehat{a}(\xi+\pi)|^2).
\end{aligned}
$$

This proves (3.2).

We now concretely construct filters $a^+, a^- \in l_2(\mathbb{Z})$ satisfying (3.3) and (7.1)–(7.3). For $\xi \in [0, \pi]$, we define
(7.4)
$$\widehat{a^+}(\xi+\pi) := \begin{cases} |\widehat{a}(\xi)|/\sqrt{2} & \text{if } |\widehat{a}(\xi)| = |\widehat{a}(\xi+\pi)|, \\ |\widehat{a}(\xi+\pi)| & \text{if } |\widehat{a}(\xi)| > |\widehat{a}(\xi+\pi)|, \\ 0 & \text{if } |\widehat{a}(\xi)| < |\widehat{a}(\xi+\pi)|, \end{cases} \quad \widehat{a^-}(\xi) := \begin{cases} |\widehat{a}(\xi)|/\sqrt{2} & \text{if } |\widehat{a}(\xi)| = |\widehat{a}(\xi+\pi)|, \\ 0 & \text{if } |\widehat{a}(\xi)| > |\widehat{a}(\xi+\pi)|, \\ |\widehat{a}(\xi)| & \text{if } |\widehat{a}(\xi)| < |\widehat{a}(\xi+\pi)|, \end{cases}$$

and

$$(7.5) \quad \widehat{a^+}(\xi) := e^{i\beta(\xi)}\sqrt{|\widehat{a}(\xi)|^2 - |\widehat{a^-}(\xi)|^2}, \quad \widehat{a^-}(\xi+\pi) := e^{-i\beta(\xi)}\sqrt{|\widehat{a}(\xi+\pi)|^2 - |\widehat{a^+}(\xi+\pi)|^2},$$

where $\beta(\xi)$ denotes the phase of $\widehat{a}(\xi)\overline{\widehat{a}(\xi+\pi)}$, that is, β is a real-valued measurable function on $[0, \pi]$ such that

$$(7.6) \qquad\qquad \widehat{a}(\xi)\overline{\widehat{a}(\xi+\pi)} = e^{i\beta(\xi)}|\widehat{a}(\xi)\overline{\widehat{a}(\xi+\pi)}|, \qquad \xi \in [0, \pi].$$

If $\widehat{a}(\xi)\overline{\widehat{a}(\xi+\pi)} = 0$, then we simply define $\beta(\xi) = 0$.

We now prove that $\widehat{a^+}(\xi)$ and $\widehat{a^-}(\xi+\pi)$ in (7.5) are well defined and all the conditions in (3.3) and (7.1)–(7.3) are satisfied. Let $\xi \in [0, \pi]$ be arbitrarily fixed. We now consider three cases.

Case 1: $|\widehat{a}(\xi)| = |\widehat{a}(\xi+\pi)|$. By (7.4), we have

$$\widehat{a^+}(\xi+\pi) = |\widehat{a}(\xi)|/\sqrt{2} = |\widehat{a}(\xi+\pi)|/\sqrt{2}, \qquad \widehat{a^-}(\xi) = |\widehat{a}(\xi)|/\sqrt{2}.$$

The above identities imply that $\widehat{a^+}(\xi)$ and $\widehat{a^-}(\xi+\pi)$ in (7.5) are well defined. More explicitly,

$$\widehat{a^+}(\xi) = e^{i\beta(\xi)}\sqrt{|\widehat{a}(\xi)|^2 - |\widehat{a^-}(\xi)|^2} = e^{i\beta(\xi)}|\widehat{a}(\xi)|/\sqrt{2}$$

and

$$\widehat{a^-}(\xi+\pi) = e^{-i\beta(\xi)}\sqrt{|\widehat{a}(\xi+\pi)|^2 - |\widehat{a^+}(\xi+\pi)|^2} = e^{-i\beta(\xi)}|\widehat{a}(\xi+\pi)|/\sqrt{2}.$$

Using the definition of β in (7.6), we can directly check that all of (3.3) and (7.1)–(7.3) are satisfied.

Case 2: $|\widehat{a}(\xi)| > |\widehat{a}(\xi+\pi)|$. By (7.4), we have

$$\widehat{a^+}(\xi+\pi) = |\widehat{a}(\xi+\pi)|, \qquad \widehat{a^-}(\xi) = 0.$$

The above identities imply that $\widehat{a^+}(\xi)$ and $\widehat{a^-}(\xi+\pi)$ in (7.5) are well defined. More explicitly,

$$\widehat{a^+}(\xi) = e^{i\beta(\xi)}\sqrt{|\widehat{a}(\xi)|^2 - |\widehat{a^-}(\xi)|^2} = e^{i\beta(\xi)}|\widehat{a}(\xi)|,$$

$$\widehat{a^-}(\xi+\pi) = e^{-i\beta(\xi)}\sqrt{|\widehat{a}(\xi+\pi)|^2 - |\widehat{a^+}(\xi+\pi)|^2} = 0.$$

By (7.6), we can directly check that all of (3.3) and (7.1)–(7.3) are satisfied.

Case 3: $|\widehat{a}(\xi)| < |\widehat{a}(\xi + \pi)|$. This case is similar to Case 2. By (7.4), we have

$$\widehat{a^+}(\xi + \pi) = 0, \qquad \widehat{a^-}(\xi) = |\widehat{a}(\xi)|.$$

The above identities imply that $\widehat{a^+}(\xi)$ and $\widehat{a^-}(\xi + \pi)$ in (7.5) are well defined. More explicitly,

$$\widehat{a^+}(\xi) = e^{i\beta(\xi)}\sqrt{|\widehat{a}(\xi)|^2 - |\widehat{a^-}(\xi)|^2} = 0,$$

$$\widehat{a^-}(\xi + \pi) = e^{-i\beta(\xi)}\sqrt{|\widehat{a}(\xi + \pi)|^2 - |\widehat{a^+}(\xi + \pi)|^2} = e^{-i\beta(\xi)}|\widehat{a}(\xi + \pi)|.$$

By (7.6), we can directly check that all of (3.3) and (7.1)–(7.3) are satisfied.

Suppose that in addition a is real valued. Then $\overline{\widehat{a}(-\xi)} = \widehat{a}(\xi)$ and consequently $|\widehat{a}(-\xi)| = |\widehat{a}(\xi)|$. Proving $\widehat{a^-}(\xi) = \overline{\widehat{a^+}(-\xi)}$ defined in (7.4) and (7.5) is equivalent to showing that

$$(7.7) \qquad \overline{\widehat{a^+}(-\xi)} = \widehat{a^-}(\xi) \quad \text{and} \quad \overline{\widehat{a^+}(\pi - \xi)} = \widehat{a^-}(\xi - \pi), \qquad a.e.\, \xi \in [0, \pi].$$

By the definition of a^+ in (7.4), for $\xi \in [0, \pi]$, we deduce that $\pi - \xi \in [0, \pi]$ and

$$\overline{\widehat{a^+}(-\xi)} = \overline{\widehat{a^+}((\pi - \xi) + \pi)} = \begin{cases} |\widehat{a}(\pi - \xi)|/\sqrt{2} = |\widehat{a}(-\xi)|/\sqrt{2} & \text{if } |\widehat{a}(\pi - \xi)| = |\widehat{a}(-\xi)|, \\ |\widehat{a}(-\xi)| & \text{if } |\widehat{a}(\pi - \xi)| > |\widehat{a}(-\xi)|, \\ 0 & \text{if } |\widehat{a}(\pi - \xi)| < |\widehat{a}(-\xi)|, \end{cases}$$

which agrees with $\widehat{a^-}(\xi)$ defined in (7.4) by $|\widehat{a}(-\xi)| = |\widehat{a}(\xi)|$ and $|\widehat{a}(\pi - \xi)| = |\widehat{a}(\xi + \pi)|$. This proves the first identity in (7.7).

For $\xi \in [0, \pi]$, we have $\pi - \xi \in [0, \pi]$ and by the definition of a^+ in (7.5),

$$(7.8) \qquad \begin{aligned} \overline{\widehat{a^+}(\pi - \xi)} &= e^{-i\beta(\pi - \xi)}\sqrt{|\widehat{a}(\pi - \xi)|^2 - |\widehat{a^-}(\pi - \xi)|^2} \\ &= e^{-i\beta(\pi - \xi)}\sqrt{|\widehat{a}(\xi + \pi)|^2 - |\widehat{a^+}(\xi + \pi)|^2}, \end{aligned}$$

where we used $|\widehat{a}(\pi - \xi)| = |\widehat{a}(\xi + \pi)|$ and the first proved identity in (7.7) with ξ being replaced by $\pi - \xi$. Replacing ξ by $\pi - \xi$ in the definition of $\beta(\xi)$ in (7.6) and using $\widehat{a}(\xi) = \overline{\widehat{a}(-\xi)}$, we have

$$e^{i\beta(\pi - \xi)}|\widehat{a}(\xi)\overline{\widehat{a}(\xi + \pi)}| = e^{i\beta(\pi - \xi)}|\widehat{a}(\pi - \xi)\overline{\widehat{a}(2\pi - \xi)}| = \widehat{a}(\pi - \xi)\overline{\widehat{a}(2\pi - \xi)}$$
$$= \overline{\widehat{a}(\xi - \pi)}\,\widehat{a}(-\xi) = \overline{\widehat{a}(\xi + \pi)}\widehat{a}(\xi) = \widehat{a}(\xi)\overline{\widehat{a}(\xi + \pi)} = e^{i\beta(\xi)}|\widehat{a}(\xi)\overline{\widehat{a}(\xi + \pi)}|.$$

Therefore, we must have $e^{i\beta(\pi - \xi)} = e^{i\beta(\xi)}$ for $\xi \in [0, \pi]$ such that $\widehat{a}(\xi)\overline{\widehat{a}(\xi + \pi)} \neq 0$. Since we defined $\beta(\xi) = 0$ when $\widehat{a}(\xi)\overline{\widehat{a}(\xi + \pi)} = 0$, we conclude that $e^{i\beta(\pi - \xi)} = e^{i\beta(\xi)}$ for all $\xi \in [0, \pi]$. Now it follows from (7.8) and (7.4) that the second identity in (7.7) must hold. This proves that the particularly constructed filters a^+ and a^- in (7.4) and (7.5) indeed satisfy $a^- = \overline{a^+}$ when a is a real-valued filter. ∎

For a finitely supported sequence $u = \{u(k)\}_{k \in \mathbb{Z}} \in l_0(\mathbb{Z})$ and $\gamma \in \mathbb{Z}$, we define its coset sequence $u^{[\gamma]}$ to be $u^{[\gamma]}(k) := u(\gamma + 2k), k \in \mathbb{Z}$, and define the Laurent polynomial $\mathsf{u}(z) := \sum_{k \in \mathbb{Z}} u(k)z^k$ and $\mathsf{u}^\star(z) := (\mathsf{u}(z))^\star := \sum_{k \in \mathbb{Z}} \overline{u(k)}^\mathsf{T} z^{-k}$ for $z \in \mathbb{C}\backslash\{0\}$.

Proof of Theorem 3.2. Sufficiency. (3.5) implies

$$|\widehat{a^+}(\xi)|^2 + |\widehat{a^-}(\xi)|^2 = |\widehat{a}(\xi)|^2(|\widehat{u^+}(2\xi)|^2 + |\widehat{u^-}(2\xi)|^2) = |\widehat{a}(\xi)|^2$$

and

$$\widehat{a^+}(\xi)\overline{\widehat{a^+}(\xi+\pi)} + \widehat{a^-}(\xi)\overline{\widehat{a^-}(\xi+\pi)} = \widehat{a}(\xi)\overline{\widehat{a}(\xi+\pi)}\left(|\widehat{u^+}(2\xi)|^2 + |\widehat{u^-}(2\xi)|^2\right) = \widehat{a}(\xi)\overline{\widehat{a}(\xi+\pi)}.$$

Hence, (3.1) holds. If in addition a is real valued and $u^- = \overline{u^+}$, then $\overline{\widehat{a}(-\xi)} = \widehat{a}(\xi)$ and $\overline{\widehat{u^+}(-\xi)} = \widehat{u^-}(\xi)$. Thus we can see that $\overline{a^+} = a^-$, since $\overline{\widehat{a^+}(-\xi)} = \overline{\widehat{a}(-\xi)}\widehat{u^+}(-2\xi) = \widehat{a}(\xi)\widehat{u^-}(2\xi) = \widehat{a^-}(\xi)$.

Necessity. Rewriting (3.1) in terms of matrices, we have

$$(7.9) \qquad \begin{bmatrix} \widehat{a^+}(\xi) & \widehat{a^-}(\xi) \\ \widehat{a^+}(\xi+\pi) & \widehat{a^-}(\xi+\pi) \end{bmatrix} \begin{bmatrix} \overline{\widehat{a^+}(\xi)} & \overline{\widehat{a^+}(\xi+\pi)} \\ \overline{\widehat{a^-}(\xi)} & \overline{\widehat{a^-}(\xi+\pi)} \end{bmatrix} = \begin{bmatrix} |\widehat{a}(\xi)|^2 & \widehat{a}(\xi)\overline{\widehat{a}(\xi+\pi)} \\ \overline{\widehat{a}(\xi)}\widehat{a}(\xi+\pi) & |\widehat{a}(\xi+\pi)|^2 \end{bmatrix}.$$

Since a is a finitely supported filter, using coset sequences and Laurent polynomials, we have $\mathsf{a}(z) = \mathsf{a}^{[0]}(z^2) + z\mathsf{a}^{[1]}(z^2)$ and $\mathsf{a}(-z) = \mathsf{a}^{[0]}(z^2) - z\mathsf{a}^{[1]}(z^2)$. Therefore, we observe that

$$\begin{bmatrix} \mathsf{a}^+(z) & \mathsf{a}^-(z) \\ \mathsf{a}^+(-z) & \mathsf{a}^-(-z) \end{bmatrix} = \mathsf{W}(z)\mathsf{V}(z^2), \qquad \begin{bmatrix} \mathsf{a}(z) & 0 \\ \mathsf{a}(-z) & 0 \end{bmatrix} = \mathsf{W}(z)\mathring{\mathsf{V}}(z^2),$$

where

$$\mathsf{W}(z) = \begin{bmatrix} 1 & z \\ 1 & -z \end{bmatrix}, \qquad \mathsf{V}(z) := \begin{bmatrix} \mathsf{a}^{+,[0]}(z) & \mathsf{a}^{-,[0]}(z) \\ \mathsf{a}^{+,[1]}(z) & \mathsf{a}^{-,[1]}(z) \end{bmatrix}, \qquad \mathring{\mathsf{V}}(z) := \begin{bmatrix} \mathsf{a}^{[0]}(z) & 0 \\ \mathsf{a}^{[1]}(z) & 0 \end{bmatrix}.$$

Hence, in terms of Laurent polynomials, we conclude that (7.9) can be rewritten as

$$\mathsf{W}(z)\mathsf{V}(z^2)\mathsf{V}^\star(z^2)\mathsf{W}^\star(z) = \mathsf{W}(z)\mathring{\mathsf{V}}(z^2)\mathring{\mathsf{V}}^\star(z^2)\mathsf{W}^\star(z).$$

Since $\det(\mathsf{W}(z)) = -2z \neq 0$ for all $z \in \mathbb{C}\backslash\{0\}$, we deduce from the above identity that

$$\mathsf{V}(z)\mathsf{V}^\star(z) = \mathring{\mathsf{V}}(z)\mathring{\mathsf{V}}^\star(z) =: \begin{bmatrix} \mathsf{p}_1(z) & \mathsf{p}_2(z) \\ \mathsf{p}_3(z) & \mathsf{p}_4(z) \end{bmatrix}$$

with $\mathsf{p}_1(z) := \mathsf{a}^{[0]}(z)(\mathsf{a}^{[0]}(z))^\star$, $\mathsf{p}_2(z) := \mathsf{a}^{[0]}(z)(\mathsf{a}^{[1]}(z))^\star$, $\mathsf{p}_3(z) := \mathsf{a}^{[1]}(z)(\mathsf{a}^{[0]}(z))^\star$, and $\mathsf{p}_4(z) := \mathsf{a}^{[1]}(z)(\mathsf{a}^{[1]}(z))^\star$. Since $\mathsf{a}(z)$ and $\mathsf{a}(-z)$ have no common zeros in $\mathbb{C}\backslash\{0\}$, by $\mathsf{a}(z) = \mathsf{a}^{[0]}(z^2) + z\mathsf{a}^{[1]}(z^2)$, we see that $\mathsf{a}^{[0]}(z)$ and $\mathsf{a}^{[1]}(z)$ have no common zeros in $\mathbb{C}\backslash\{0\}$. Consequently, by the definition of $\mathsf{p}_1, \mathsf{p}_2, \mathsf{p}_3$, and p_4, there does not exist $z_0 \in \mathbb{C}\backslash\{0\}$ such that $\mathsf{p}_1(z_0) = \mathsf{p}_2(z_0) = \mathsf{p}_3(z_0) = \mathsf{p}_4(z_0)$. That is, all the Laurent polynomials $\mathsf{p}_1, \mathsf{p}_2, \mathsf{p}_3$, and p_4 have no common zeros in $\mathbb{C}\backslash\{0\}$. It is obvious that $\det(\mathring{\mathsf{V}}(z)) = 0$. Consequently, we have $\det(\mathsf{V}(z)) = 0$ since $\det(\mathsf{V}(z))(\det(\mathsf{V}(z)))^\star = \det(\mathring{\mathsf{V}}(z))(\det(\mathring{\mathsf{V}}(z)))^\star = 0$. Now by [23, Theorem 3.6], there exists a 2×2 matrix U of Laurent polynomials such that

$$(7.10) \qquad \mathsf{U}(z)\mathsf{U}^\star(z) = I_2 \quad \text{and} \quad \mathsf{V}(z) = \mathring{\mathsf{V}}(z)\mathsf{U}(z) \quad \text{with} \quad \mathsf{U}(z) = \begin{bmatrix} \mathsf{u}^+(z) & \mathsf{u}^-(z) \\ \mathsf{u}_1(z) & \mathsf{u}_2(z) \end{bmatrix}.$$

The second identity in (7.10) can be rewritten as

$$\mathsf{a}^{+,[0]}(z) = \mathsf{a}^{[0]}(z)\mathsf{u}^+(z), \quad \mathsf{a}^{+,[1]}(z) = \mathsf{a}^{[1]}(z)\mathsf{u}^+(z),$$
$$\mathsf{a}^{-,[0]}(z) = \mathsf{a}^{[0]}(z)\mathsf{u}^-(z), \quad \mathsf{a}^{-,[1]}(z) = \mathsf{a}^{[1]}(z)\mathsf{u}^-(z).$$

Therefore, by $\mathsf{a}(z) = \mathsf{a}^{[0]}(z^2) + z\mathsf{a}^{[1]}(z^2)$, we have

$$\mathsf{a}^+(z) = \mathsf{a}^{+,[0]}(z^2) + z\mathsf{a}^{+,[1]}(z^2) = \mathsf{a}^{[0]}(z^2)\mathsf{u}^+(z^2) + z\mathsf{a}^{[1]}(z^2)\mathsf{u}^+(z^2) = \mathsf{a}(z)\mathsf{u}^+(z^2)$$

and similarly $\mathsf{a}^-(z) = \mathsf{a}^{-,[0]}(z^2) + z\mathsf{a}^{-,[1]}(z^2) = \mathsf{a}(z)\mathsf{u}^-(z^2)$. That is, the first two identities in (3.5) hold. The first identity in (7.10) implies $\mathsf{u}^+(z)(\mathsf{u}^+(z))^\star + \mathsf{u}^-(z)(\mathsf{u}^-(z))^\star = 1$, which is the third identity in (3.5). This proves the necessity part.

If in addition a is real valued and $a^- = \overline{a^+}$, we have $\widehat{a}(-\xi) = \overline{\widehat{a}(\xi)}$ and we deduce from (3.5) that

$$\widehat{a}(\xi)\widehat{u^-}(2\xi) = \widehat{a^-}(\xi) = \overline{\widehat{a^+}(-\xi)} = \overline{\widehat{a}(-\xi)}\,\overline{\widehat{u^+}(-2\xi)} = \widehat{a}(\xi)\overline{\widehat{u^+}(-2\xi)},$$

from which we must have $\widehat{u^-}(\xi) = \overline{\widehat{u^+}(-\xi)}$, since $\widehat{a}$ is not identically zero (otherwise, all $z \in \mathbb{C}\backslash\{0\}$ will be common zeros of $\mathsf{a}(z)$ and $\mathsf{a}(-z)$). This proves $u^- = \overline{u^+}$. Conversely, since a is real valued, it follows directly from $u^- = \overline{u^+}$ and (3.5) that $a^- = \overline{a^+}$. ∎

Proof of Theorem 3.3. By the definition of $\mathsf{P}_{m,\ell}$ in (3.9) and $c > 0$, we have

$$\ell\mathsf{P}_{m,\ell}(c) - c\mathsf{P}'_{m,\ell}(c) = \ell\sum_{j=0}^{\ell-1}\binom{m+j-1}{j}c^j - c\sum_{j=1}^{\ell-1}\binom{m+j-1}{j}jc^{j-1}$$

$$= \ell + \sum_{j=1}^{\ell-1}\binom{m+j-1}{j}(\ell-j)c^j \geqslant \ell > 0.$$

Now we can deduce that $c_0 < 0$. By the above inequality and $2 - 1/c \geqslant 0$, we have

$$(2+2\ell-\ell/c)\mathsf{P}_{m,\ell}(c)+(1-2c)\mathsf{P}'_{m,\ell}(c) = 2\mathsf{P}_{m,\ell}(c)+(2-1/c)(\ell\mathsf{P}_{m,\ell}(c)-c\mathsf{P}'_{m,\ell}(c)) \geqslant 2\mathsf{P}_{m,\ell}(c) > 0.$$

This proves $c_1 > 0$.

Note that the parameters c_0 and c_1 in (3.14) are chosen so that both $\mathsf{P}(c) = 0$ and $\mathsf{P}'(c) = 0$. Since P is a polynomial of degree $\ell+1$ and $\mathsf{P}(c) = \mathsf{P}'(c) = 0$, we can write $\mathsf{P}(x) = (1-\frac{x}{c})^2\mathsf{Q}(x)$ for some unique polynomial Q of degree $\ell-1$. Note that $\mathsf{P}_{m,\ell}$ in (3.9) is the $(\ell-1)$th-degree Taylor polynomial of $\frac{1}{(1-x)^m}$ at the point $x = 0$. By the definition of P in (3.13), we deduce that $\mathsf{Q}(z) = (1-\frac{x}{c})^{-2}\mathsf{P}_{m,\ell}(x) + x^\ell(c_0 - (c_1+2c_0)x)(1-\frac{x}{c})^{-2}$, from which we conclude that Q must be the $(\ell-1)$th-degree Taylor polynomial of $\frac{1}{(1-x)^m(1-\frac{x}{c})^2}$ at the point $x = 0$. Consequently, all the coefficients of Q are nonnegative. Therefore, $\mathsf{P}(x) = (1-\frac{x}{c})^2\mathsf{Q}(x) \geqslant 0$ for all $x \geqslant 0$. In particular, $\mathsf{P}(x) \geqslant 0$ for all $x \in [0, 1]$.

By the definition of P in (3.13), we have

$$(7.11) \qquad 1 - (1-x)^m\mathsf{P}(x) - x^m\mathsf{P}(1-x) = 1 - (1-x)^m\mathsf{P}_{m,\ell}(x) - x^m\mathsf{P}_{m,\ell}(1-x) + \mathsf{R}(x)$$

with $\mathsf{R}(x) := c_0(x^m(1-x)^\ell - (1-x)^m x^\ell)(1-2x) + c_1((1-x)^m x^{\ell+1} + x^m(1-x)^{\ell+1})$. Since $1 \leqslant \ell \leqslant m$, we have

$$(x^m(1-x)^\ell - (1-x)^m x^\ell)(1-2x) = x^\ell(1-x)^\ell(x^{m-\ell} - (1-x)^{m-\ell})(1-2x) \leqslant 0 \quad \forall\, x \in [0,1].$$

Since $c_0 < 0$ and $c_1 > 0$, we conclude from (7.11) that $\mathsf{R}(x) \geqslant 0$ for all $x \in [0,1]$ and

$$\begin{aligned}
1 - (1-x)^m \mathsf{P}(x) - x^m \mathsf{P}(1-x) &\geqslant 1 - (1-x)^m \mathsf{P}_{m,\ell}(x) - x^m \mathsf{P}_{m,\ell}(1-x) \\
&\geqslant 1 - (1-x)^m \mathsf{P}_{m,m}(x) - x^m \mathsf{P}_{m,m}(1-x) = 0,
\end{aligned}$$

where we used $(1-x)^m \mathsf{P}_{m,m}(x) + x^m \mathsf{P}_{m,m}(1-x) = 1$ (see [9]) and it is obvious that $\mathsf{P}_{m,\ell}(x) \leqslant \mathsf{P}_{m,m}(x)$ for all $x \geqslant 0$. This proves (3.12). ∎

REFERENCES

[1] B. G. BODMANN, G. KUTYNIOK, AND X. ZHUANG, *Gabor shearlets*, Appl. Comput. Harmon. Anal., 38 (2015), pp. 87–114.

[2] E. J. CANDÈS, AND D. L. DONOHO, *New tight frames of curvelets and optimal representations of objects with piecewise C^2 singularities*, Commun. Pure Appl. Math., 57 (2004), pp. 219–266.

[3] E. CANDÈS, L. DEMANET, D. DONOHO, AND L. YING, *Fast discrete curvelet transforms*, Multiscale Model. Simul., 5 (2006), pp. 861–899.

[4] E. J. CANDÈS AND D. L. DONOHO, *Ridgelets: A key to higher-dimensional intermittency?*, Philos. Trans. Roy. Soc. A, 357 (1999), pp. 2495–2509.

[5] Z. CHE AND X. ZHUANG, *Digital affine shear filter banks with 2-layer structure and their applications in image processing*, IEEE Trans. Image Process., 27 (2018), pp. 3931–3941.

[6] C. K. CHUI, *An Introduction to Wavelets*, Academic Press, New York, 1992.

[7] C. K. CHUI, W. HE, AND J. STÖCKLER, *Compactly supported tight and sibling frames with maximum vanishing moments*, Appl. Comput. Harmon. Anal., 13 (2002), pp. 224–262.

[8] K. DABOV, A. FOI, V. KATKOVNIK, AND K. EGIAZARIAN, *Image denoising by sparse 3D transform-domain collaborative filtering*, IEEE Trans. Image Process., 16 (2007), pp. 3736–3745.

[9] I. DAUBECHIES, *Ten Lectures on Wavelets*, CBMS-NSF Regional Conf. Ser. in Appl. Math. 61, SIAM, Philadelphia, 1992.

[10] I. DAUBECHIES, B. HAN, A. RON, AND Z. SHEN, *Framelets: MRA-based constructions of wavelet frames*, Appl. Comput. Harmon. Anal., 14 (2003), pp. 1–46.

[11] B. DONG AND Z. SHEN, *MRA-based wavelet frames and applications*, in Mathematics in Image Processing, IAS/Park City Math. Ser., 19, American Mathematical Society, Providence, RI, 2010, pp. 7–158.

[12] D. L. DONOHO, G. KUTYNIOK, M. SHAHRAM, AND X. ZHUANG, *A rational design of a digital shearlet transform*, in the 9th International Conference on Sampling Theory and Applications (SampTA'11), Singapore, 2011.

[13] G. EASLEY, D. LABATE, AND W.-Q. LIM, *Sparse directional image representations using the discrete shearlet transform*, Appl. Comput. Harmon. Anal., 25 (2008), pp. 25–46.

[14] K. GUO, G. KUTYNIOK, AND D. LABATE, *Sparse multidimensional representations using anisotropic dilation and shear operators*, Wavelets and Splines (Athens, GA, 2005), Nashboro Press, Nashville, TN, 2006, pp. 189–201.

[15] K. GUO, D. LABATE, W.-Q. LIM, G. WEISS, AND E. N. WILSON, *Wavelets with composite dilations*, Electron. Res. Announc. Amer. Math. Soc., 10 (2004), pp. 78–87.

[16] B. HAN, *On dual wavelet tight frames*, Appl. Comput. Harmon. Anal., 4 (1997), pp. 380–413.

[17] B. HAN, *Symmetric orthonormal complex wavelets with masks of arbitrarily high linear-phase moments and sum rules*, Adv. Comput. Math., 32 (2010), pp. 209–237.

[18] B. HAN, *Nonhomogeneous wavelet systems in high dimensions*, Appl. Comput. Harmon. Anal., 32 (2012), pp. 169–196.

[19] B. HAN, *Properties of discrete framelet transforms*, Math. Model. Nat. Phenom., 8 (2013), pp. 18–47.

[20] B. HAN, *Symmetric tight framelet filter banks with three high-pass filters*, Appl. Comput. Harmon. Anal., 37 (2014), pp. 140–161.

[21] B. HAN, *Algorithm for constructing symmetric dual framelet filter banks*, Math. Comp., 84 (2015), pp. 767–801.

[22] B. HAN, *Framelets and Wavelets: Algorithms, Analysis, and Applications*, Appl. Numer. Harmon. Anal., Birkhäuser, Cham, Switzerland, 2017.

[23] B. HAN, Q. MO, AND Z. ZHAO, *Compactly supported tensor product complex tight framelets with directionality*, SIAM J. Math. Anal., 47 (2015), pp. 2464–2494.

[24] B. HAN AND Z. ZHAO, *Tensor product complex tight framelets with increasing directionality*, SIAM J. Imaging Sci., 7 (2014), pp. 997–1034.

[25] B. HAN, Z. ZHAO, AND X. ZHUANG, *Directional tensor product complex tight framelets with low redundancy*, Appl. Comput. Harmon. Anal., 41 (2016), pp. 603–637.

[26] B. HAN AND X. ZHUANG, *Smooth affine shear tight frames with MRA structure*, Appl. Comput. Harmon. Anal., 39 (2015), pp. 300–338.

[27] S. HÄUSER AND G. STEIDL, *Convex multiclass segmentation with shearlet regularization*, Int. J. Comput. Math., 90 (2013), pp. 62–81.

[28] N. G. KINGSBURY, *Complex wavelets for shift invariant analysis and filtering of signals*, Appl. Comput. Harmon. Anal., 10 (2001), pp. 234–253.

[29] G. KUTYNIOK AND D. LABATE, *Shearlets: Multiscale Analysis for Multivariate Data*, Birkhäuser, Boston, 2012.

[30] G. KUTYNIOK, W.-Q. LIM, AND R. REISENHOFER, *ShearLab 3D: Faithful digital shearlet transforms based on compactly supported shearlets*, ACM Trans. Math. Software, 42 (2016), 5.

[31] G. KUTYNIOK, M. SHAHRAM, AND X. ZHUANG, *ShearLab: A rational design of a digital parabolic scaling algorithm*, SIAM J. Imaging Sci., 5 (2012), pp. 1291–1332.

[32] M. LEBRUN, *An analysis and implementation of the BM3D image denoising method*, IPOL J. Image Process. Online, 2 (2012), pp. 175–213.

[33] Y.-R. LI, L. SHEN, AND B. W. SUTER, *Adaptive inpainting algorithm based on DCT induced wavelet regularization*, IEEE Trans. Image Process., 22 (2013), pp. 752–763.

[34] W.-Q LIM, *The discrete shearlet transform: A new directional transform and compactly supported shearlet frames*, IEEE Trans. Image Process., 19 (2010), pp. 1166–1180.

[35] W.-Q LIM, *Nonseparable shearlet transform*, IEEE Trans. Image Process., 22 (2013), pp. 2056–2065.

[36] A. RON AND Z. SHEN, *Affine systems in $L_2(\mathbb{R}^d)$: The analysis of the analysis operator*, J. Funct. Anal., 148 (1997), pp. 408–447.

[37] I. W. SELESNICK, R. G. BARANIUK, AND N. G. KINGSBURY, *The dual-tree complex wavelet transform*, IEEE Signal Process. Mag., 22 (2005), pp. 123–151.

[38] L. SENDUR AND I. W. SELESNICK, *Bivariate shrinkage with local variance estimation*, IEEE Signal Process. Lett., 9 (2002), pp. 438–441.

[39] Y. SHEN, B. HAN, AND E. BRAVERMAN, *Image inpainting from partial noisy data by directional complex tight framelets*, ANZIAM J., 58 (2017), pp. 247–255.

[40] E. P. SIMONCELLI, W. T. FREEMAN, E. H. ADELSON, AND D. J. HEEGER, *Shiftable multiscale transforms*, IEEE Trans. Inform. Theory, 38 (1992), pp. 587–607.

[41] J.-L. STARCK, E. J. CANDÈS, AND D. L. DONOHO, *The curvelet transform for image denoising*, IEEE Trans. Image Process., 11 (2002), pp. 670–684.

[42] X. ZHUANG, *Digital affine shear transforms: Fast realization and applications in image/video processing*, SIAM J. Imaging Sci., 9 (2016), pp. 1437–1466.